



**FRIEDRICH-SCHILLER-  
UNIVERSITÄT  
JENA**

Bachelorarbeit zur Erlangung des akademischen Grades  
Bachelor of Science in Physik

---

Characterization of optical components  
of a laser amplifier via spectral interferometry

---

Martin Beyer

geboren am 22. Juni 1999 in Weimar

Gutachter:

Prof. Dr. Malte C. Kaluza

Dr. Sebastian Keppler

30. September 2020

# Contents

<b>1. Introduction</b>	<b>1</b>
<b>2. Fundamentals of ultrafast optics</b>	<b>2</b>
2.1. Fundamentals of electromagnetic waves	2
2.2. Gaussian beams	4
2.3. Optical pulses	5
2.4. Spectral phase and dispersion	6
<b>3. Spectral interferometry</b>	<b>10</b>
3.1. The method of spectral interferometry	10
3.2. GDD determination via phase differentiation	12
3.3. GDD determination via the cubic phase function	14
<b>4. Study of the spectral phase</b>	<b>16</b>
4.1. Experimental setup	16
4.2. The measurement procedure	17
4.3. Measurement referencing with fused silica and YAG crystal	18
4.4. Experimental issues	19
4.4.1. Spectral calibration	20
4.4.2. Spectral resolution	21
4.4.3. Noise sensitivity	24
4.4.4. Frequency sampling	25
4.4.5. Change to frequency domain	26
4.4.6. Angular chirp and pulse front tilt	27
<b>5. Characterization of a laser amplifier</b>	<b>29</b>
5.1. Setup of the laser amplifier	29
5.2. Characterization of the optical components	30
<b>6. Conclusion</b>	<b>35</b>
<b>7. List of abbreviations</b>	<b>39</b>
<b>A. Sellmeier equations of the used materials</b>	<b>40</b>
<b>B. Characterization of Glan-type polarizers</b>	<b>41</b>
<b>C. The LabVIEW application</b>	<b>42</b>
<b>D. Deflection angle of a prism</b>	<b>44</b>

# 1. Introduction

One of the largest branches of modern optics is laser technology, which offers a wide range of applications in industry, medicine and research. In particular, the generation of sub-picosecond laser pulses has greatly expanded the possibilities for the application of laser systems. An important milestone in the development of pulsed laser systems was the chirped pulse amplification (CPA) principle developed by STRICKLAND and MOUROU in 1985 [1], which earned them the Nobel Prize in 2018. The high peak powers that can be achieved by lasers employing the CPA schemes are used e.g. for experiments aiming at laser-driven proton acceleration. Such experiments are performed at the high intensity laser system POLARIS (Petawatt Optical Laser Amplifier for Radiation Intensive Experiments) which is operated at the Helmholtz Institute Jena. In order to characterize the plasma conditions during such experiments very precisely, an independent pump-probe setup is currently being developed. With this setup the precise characterization of the formation and temporal evolution of the plasma target becomes possible. For the plasma characterization setup, a CPA system consisting of a pulse stretcher, regenerative amplifier and pulse compressor is being developed.

In order to characterize the pre-plasma, knowledge of the temporal shape of the laser pulse is important. One of the main big issues is the measurement of ultra short laser pulses with durations of 50 fs, which is shorter than the response time of any electronic detector. In order to measure such kind of laser pulses, a reference pulse with a comparable duration can be used to sample the pulse to be measured by a suitable detector. Such a sample pulse can be the pulse itself or another well characterized femtosecond laser pulse [2]. It is important to measure both amplitude and phase of the spectrum, although it is usually not possible to measure the latter directly. One of the most effective methods of laser pulse characterization is called spectral interferometry (SI) which was pioneered by FROEHLY et al. in 1973 [3]. It offers the possibility to measure the spectral phase and has attracted the attention of researchers because of its large sensitivity and high spectral resolution. SI has many applications in spectroscopy [4], plasma probing [5], characterization of dispersion, studies of nonlinear processes [6], materials and characterization of crystals [7]. SI is also the basis for new techniques of spectral phase measurement, such as frequency resolved optical gating (FROG) [2] or spectral phase interferometry for direct electric field construction (SPIDER) [8].

In section 2 of this Bachelor thesis, the fundamentals of ultrafast optics based on MAXWELL's equations are presented, Gaussian beams, optical pulses and their propagation in dispersive media are introduced. The method of spectral interferometry (SI) is fundamentally introduced and explained in section 3, different possibilities for characterizing the spectral phase are presented. The experimental setup for the characterization and a referencing measurement to well characterized materials is done in section 4. It is also investigated in section 4 which experimental issues can occur, how large their influences on the measurement are and how they can be resolved. The derived methods of spectral phase characterization are used in section 5 to specify the optical components of an amplifier in a CPA laser system. The components of the laser amplifier are categorized and their effects on the spectral phase are compared and discussed. It is then summarized why dispersion measurements are important and how the method of SI can be utilized to select suitable components for a laser amplifier.

## 2. Fundamentals of ultrafast optics

In order to understand the technique of SI and its fields of application, a basic understanding of the fundamentals of ultrashort pulses is required. At first, electromagnetic waves and their propagation are introduced, which are the basis of all kinds of laser radiation. Subsequently, the spatial and temporal properties of laser radiation and especially the propagation of ultrashort pulses are described. The propagation of laser pulses in a material is subject to dispersion depending on the refractive index  $n(\lambda)$  of the medium which is a function of the wavelength  $\lambda$ . The dispersion is characterized by the spectral phase, which can be retrieved by measuring the spectral interference of two pulses, which appears as fringes in the spectrum.

### 2.1. Fundamentals of electromagnetic waves

All kinds of electromagnetic radiation can be described by MAXWELL's equations. These are a set of relationships between the electric field  $\mathbf{E}(\mathbf{r}, t)$  and magnetic flux density  $\mathbf{B}(\mathbf{r}, t)$ . Inside a medium the fields affect the bound charges and currents of the material which lead to the displacement field  $\mathbf{D}(\mathbf{r}, t)$ . Using these fields MAXWELL's equations can be written as follows [9]

$$\nabla \cdot \mathbf{D}(\mathbf{r}, t) = \varrho \quad (2.1a)$$

$$\nabla \cdot \mathbf{B}(\mathbf{r}, t) = 0 \quad (2.1b)$$

$$\nabla \times \mathbf{E}(\mathbf{r}, t) = -\frac{\partial}{\partial t} \mathbf{B}(\mathbf{r}, t) \quad (2.1c)$$

$$\nabla \times \mathbf{H}(\mathbf{r}, t) = \mathbf{j}(\mathbf{r}, t) + \frac{\partial}{\partial t} \mathbf{D}(\mathbf{r}, t). \quad (2.1d)$$

The quantities  $\varrho(\mathbf{r}, t)$  and  $\mathbf{j}(\mathbf{r}, t)$  are the free charge- and current densities, respectively. The displacement field  $\mathbf{D}(\mathbf{r}, t)$  and magnetic field  $\mathbf{H}(\mathbf{r}, t)$  are given by

$$\mathbf{D}(\mathbf{r}, t) = \varepsilon_0 \mathbf{E}(\mathbf{r}, t) + \mathbf{P}(\mathbf{r}, t) \quad (2.2)$$

$$\mathbf{H}(\mathbf{r}, t) = \frac{1}{\mu_0} (\mathbf{B}(\mathbf{r}, t) - \mathbf{M}(\mathbf{r}, t)). \quad (2.3)$$

The response fields of the bound charges in the medium are described by the polarization  $\mathbf{P}(\mathbf{r}, t)$  and magnetization  $\mathbf{M}(\mathbf{r}, t)$ . The field of optics is generally concerned with non-magnetizable media which means  $\mathbf{M}(\mathbf{r}, t) = 0$ .

Assuming a medium without external charges and currents ( $\varrho(\mathbf{r}, t) = 0, \mathbf{j}(\mathbf{r}, t) = 0$ ), MAXWELL's equations can be used to describe the radiation fields. Taking the curl of equation (2.1c) and subsequently using (2.1d) and (2.2) results in the *wave equation*

$$\Delta \mathbf{E}(\mathbf{r}, t) - \frac{1}{c^2} \frac{\partial^2}{\partial t^2} \mathbf{E}(\mathbf{r}, t) = \mu_0 \frac{\partial^2}{\partial t^2} \mathbf{P}(\mathbf{r}, t). \quad (2.4)$$

The polarization  $\mathbf{P}(\mathbf{r}, t)$  can be connected to the electric field via the DRUDE-LORENTZ model which assumes the material to be an ensemble of non-coupling, driven and damped

harmonic oscillators [10]. The response of the bound charges to an incident electric field can be described in the frequency domain which introduces the *susceptibility*  $\chi_{ij}(\mathbf{r}, \omega)$

$$\mathbf{P}_i(\mathbf{r}, \omega) = \varepsilon_0 \sum_j \chi_{ij}(\mathbf{r}, \omega) \mathbf{E}_j(\mathbf{r}, \omega), \quad (2.5)$$

where  $i, j = x, y, z$  are the directions in the three-dimensional space. For a linear, homogenous, isotropic and dispersive medium the susceptibility is constant in the material and depends linearly on the electric field

$$\mathbf{P}(\mathbf{r}, \omega) = \varepsilon_0 \chi(\omega) \mathbf{E}(\mathbf{r}, \omega). \quad (2.6)$$

### Plane waves and Helmholtz equation

A special form of electromagnetic radiation is a laser beam, which is characterized by its high spatial and temporal coherence properties. The laser beam is generated by stimulated emission of photons in a medium, in which the atoms are in an excited state and can release their excess energy spontaneously or stimulated by photons. The laser-active medium must be such that a population inversion of the excited states in the atoms occurs when external energy is supplied. If more photons are emitted stimulated than absorbed by the material, incident radiation can be effectively amplified. The resulting coherent laser beam can be described in the time domain with a monochromatic wave of the angular frequency  $\omega$ . The time dependence can be written in the following form

$$\mathbf{E}(\mathbf{r}, t) = \mathbf{E}_0(\mathbf{r}, t) \exp(-i\omega t), \quad (2.7)$$

where  $\mathbf{E}_0(\mathbf{r}, t)$  is the envelope of the electric field. All measurable quantities can be obtained by taking the real part of the complex components. Using (2.7), MAXWELL's equations can be expressed in the frequency domain by replacing the partial time derivative  $\frac{\partial}{\partial t}$  with  $-i\omega$  [10]. The wave equation (2.4) thus results in the HELMHOLTZ equation

$$\begin{aligned} \Delta \mathbf{E}(\mathbf{r}, \omega) + \frac{\omega^2}{c^2} \mathbf{E}(\mathbf{r}, \omega) &\stackrel{(2.6)}{=} -\omega^2 \mu_0 \varepsilon_0 \chi(\omega) \mathbf{E}(\mathbf{r}, \omega) \\ \Delta \mathbf{E}(\mathbf{r}, \omega) + \frac{\varepsilon(\omega) \omega^2}{c^2} \mathbf{E}(\mathbf{r}, \omega) &= 0 \quad \text{with} \quad \varepsilon(\omega) = 1 + \chi(\omega), \quad \frac{1}{c^2} = \mu_0 \varepsilon_0. \end{aligned} \quad (2.8)$$

The refractive index  $n(\omega)$  is defined as the ratio of the speed of light in vacuum to the speed in the medium. Equation (2.8) shows that  $c^2$  is reduced by  $\varepsilon$  which implies  $n(\omega) = \sqrt{\varepsilon(\omega)}$ .

A special solution of the wave equations (2.8) and (2.4) are *plane waves*. They describe a wave where the spatial extension of the electric field is constant over any plane perpendicular to the propagation direction

$$\mathbf{E}(\mathbf{r}, t) = \mathbf{E}_0 \exp[i(\mathbf{k} \cdot \mathbf{r} - \omega t)]. \quad (2.9)$$

Plane waves fulfill the HELMHOLTZ equation (2.8) if the dispersion relation

$$|\mathbf{k}(\omega)| = \frac{n(\omega) \omega}{c} \quad (2.10)$$

holds, which connects the absolute value of the wave vector  $\mathbf{k}(\omega)$  (its magnitude is inversely proportional to the wavelength  $\lambda$ ), to the angular frequency of the electric field.

## 2.2. Gaussian beams

In order to combine the properties of ray optics, which describe the propagation of light rays in optical systems, with wave optics, GAUSSIAN beams are introduced. In general a laser beam can be described by a continuous superposition of stationary plane waves with different wave vectors  $\mathbf{k}$  [10]

$$\mathbf{E}(\mathbf{r}, t) = \int_{\mathbb{R}^3} \mathbf{E}_0(\mathbf{k}) \exp[i(\mathbf{k} \cdot \mathbf{r} - \omega t)] d^3k. \quad (2.11)$$

GAUSSIAN beams are a solution of the HELMHOLTZ equation (2.8) and feature a special transversal shape of a two dimensional GAUSSIAN function [11]. Due to diffraction effects, the laser beam diverges during its propagation, but the GAUSSIAN shaped transversal profile remains. The complex amplitude  $E(\varrho, z)$  of the GAUSSIAN beam, expressed as a function of the propagation coordinate  $z$  and transversal coordinate  $\varrho = \sqrt{x^2 + y^2}$  can be written as [12]

$$E(\varrho, z) = E_0 \frac{w_0}{w(z)} \exp\left(-\frac{\varrho^2}{w(z)^2}\right) \exp\left[-i\left(kz + k\frac{\varrho^2}{2R(z)} + \arctan\left(\frac{z}{z_R}\right)^2\right)\right]. \quad (2.12)$$

The beam radius  $w(z)$  is defined as the distance from the propagation axis at a certain value  $z$ , at which the amplitude of the electric field is reduced to  $1/e$  of the maximum value and  $R(z)$  is the radius of curvature of the wavefront due to the divergence of the beam. They are defined as

$$w(z) = w_0 \sqrt{1 + \left(\frac{z}{z_R}\right)^2}, \quad R(z) = z \left[1 + \left(\frac{z_R}{z}\right)^2\right] \quad (2.13)$$

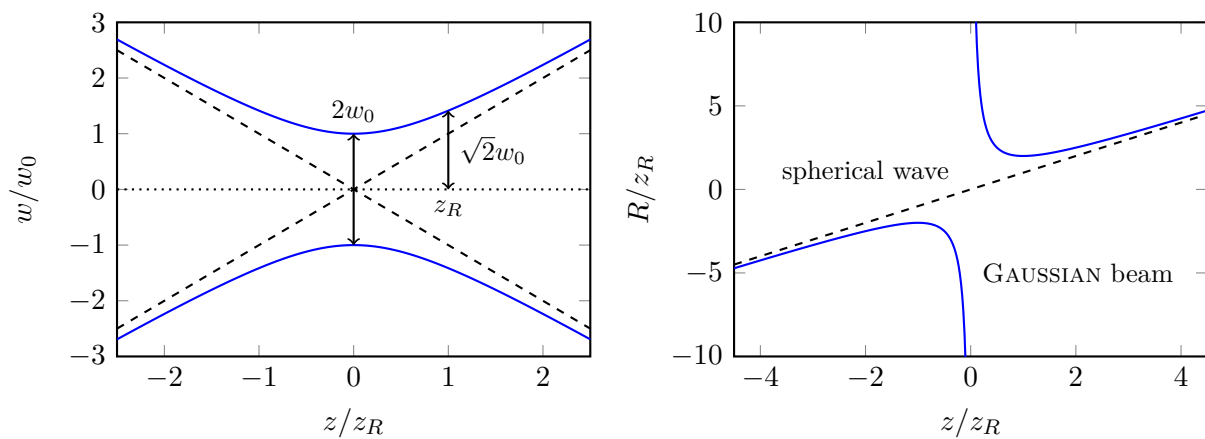


**Fig. 2.1:** Representation of beam width  $w(z)$  and radius of curvature  $R(z)$  of Gaussian beams as a function of propagation length  $z$  in units of the RAYLEIGH length  $z_R$ .

and are depicted in figure 2.1. The quantity  $z_R$  is called the RAYLEIGH length and describes the distance to the focal plane (at  $z = 0$ ) where the beam size has increased by the factor  $\sqrt{2}$ . It is defined as

$$z_R = \frac{\pi w_0^2}{\lambda}. \quad (2.14)$$

The measurable quantity of a laser beam is the intensity  $\mathbf{I}$ , a physical quantity describing energy per area and time. It can be written mathematically as the magnitude of the time averaged Poynting vector  $\mathbf{S} = \mathbf{E} \times \mathbf{H}$ , which describes the density of the energy flow. For nonmagnetic materials the intensity can be written as [9]

$$\mathbf{I} = |\langle \mathbf{E} \times \mathbf{H} \rangle| = \frac{1}{2} \varepsilon_0 c \cdot n |\mathbf{E}_0|^2. \quad (2.15)$$

Therefore the temporal intensity  $\mathbf{I}$  of a laser beam is proportional to the square of the momentary magnitude of the envelope  $\mathbf{E}_0$  of the laser beam.

### 2.3. Optical pulses

Experiments and applications that require high peak intensities instead of high average power are not feasible with continuous wave lasers. For this purpose, ultrashort laser pulses are used. Such a laser pulse is a superposition of laser beams with different frequencies  $\omega$  [10]

$$\mathbf{E}(\mathbf{r}, t) = \int_{\mathbb{R}^3} \int_{-\infty}^{\infty} \mathbf{E}_0(\mathbf{k}, \omega) \exp[i(\mathbf{k} \cdot \mathbf{r} - \omega t)] d^3k d\omega. \quad (2.16)$$

In a laser resonator of length  $L$  and effective refractive index  $n$  this is achieved via the mode locking technique which synchronizes the phase of all longitudinal modes ( $m\lambda = 2nL$  where  $m$  is an integer) [12] that can be amplified in the resonator. For a linearly polarized temporally GAUSSIAN shaped laser pulse the electric field can be written as [10]

$$\begin{aligned} \mathbf{E}(t) &= \frac{1}{2} \mathbf{E}_0 \exp(i\phi(t)) \exp\left[-\left(\frac{t}{\tau}\right)^2\right] + \text{c.c.} \\ &= \mathbf{E}_0 \cos(\phi(t)) \exp\left[-\left(\frac{t}{\tau}\right)^2\right]. \end{aligned} \quad (2.17)$$

The pulse and its envelope are shown in figure 2.2. In the frequency domain the electric field of the pulse can be described as the Fourier transform (FT) of the electric field in the time domain and vice versa

$$E(\omega) = \frac{1}{\sqrt{2\pi}} \int_{-\infty}^{\infty} E(t) \exp(-i\omega t) dt \quad (2.18)$$

$$E(t) = \frac{1}{\sqrt{2\pi}} \int_{-\infty}^{\infty} E(\omega) \exp(i\omega t) d\omega. \quad (2.19)$$

Assuming  $\phi(t) = \omega_0 t$  and substituting (2.17) into (2.18) yields

$$\mathbf{E}(\omega) = \mathbf{E}_0 \frac{\tau}{2\sqrt{2}} \left( \exp\left(-\frac{\tau^2(\omega - \omega_0)^2}{4}\right) + \exp\left(-\frac{\tau^2(\omega + \omega_0)^2}{4}\right) \right). \quad (2.20)$$

The electric field  $E(t)$  (2.17) in the time domain is assumed to be a real function, therefore it has HERMITIAN symmetry  $\mathcal{F}(E(t))(-\omega) = \mathcal{F}(E(t))^*(\omega)$  [12]. Since the spectrum (2.20) is also real, the spectrum must be symmetric for positive and negative frequencies, which means that positive and negative parts of the spectrum contain the same information. Therefore it is sufficient to consider only the positive frequency component.

Analogous to (2.15) the spectral intensity  $S(\omega)$  is defined as the square of the magnitude of the electric field in the frequency domain. According to (2.20) it can be written as

$$S(\omega) \propto |\mathbf{E}_0|^2 \exp\left(-\frac{\tau^2(\omega - \omega_0)^2}{4}\right)^2. \quad (2.21)$$

The bandwidth of the pulse and its pulse duration can be characterized by the time-bandwidth product, which can be determined by measuring the intensity full width at half maximum (FWHM)  $\Delta t$  of the pulse and of its spectrum  $\Delta\omega$ . For GAUSSIAN envelopes the bandwidth product is [9]

$$\Delta t \cdot \Delta\nu = \frac{2 \ln 2}{\pi} \approx 0.441 \quad \text{with } \Delta\nu = \frac{\Delta\omega}{2\pi}. \quad (2.22)$$

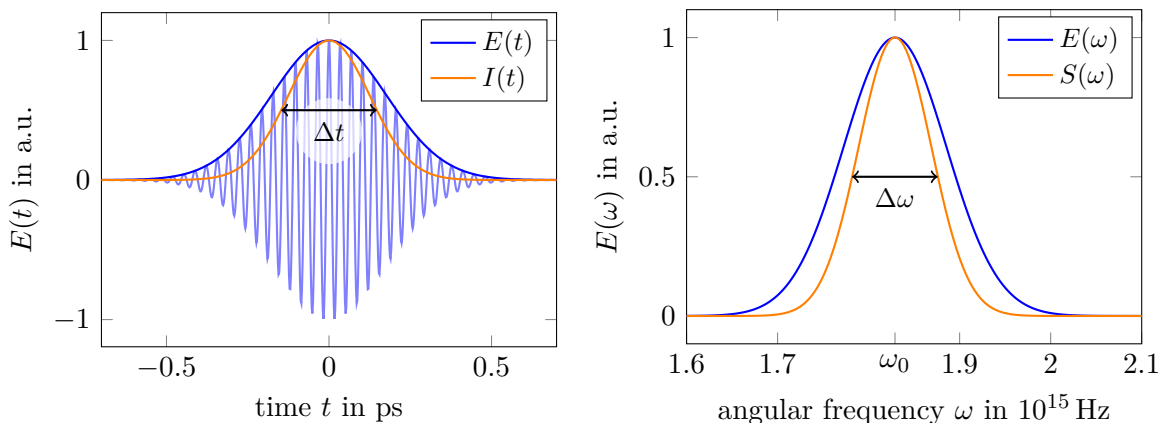


**Fig. 2.2:** Electric field (light blue) and the enveloping GAUSSIAN amplitude (blue) of a pulse with  $\tau = 25$  fs and  $\omega_0 = 1829$  THz ( $\lambda_0 = 1030$  nm). The orange curves are the temporal and spectral intensity with the FWHM criteria.

## 2.4. Spectral phase and dispersion

Until now, optical pulses have only been considered as electric fields in the time or frequency domain with a limited temporal or spectral amplitude. Now a quantity is sought which can adequately describe the change of the temporal shape during propagation through an optical medium. For this the complex FT of the temporal pulse shape according to equation (2.17) with the arbitrary phase  $\phi(t)$  is considered. The result can be separated into its spectral intensity  $S(\omega)$  and *spectral phase*  $\varphi(\omega)$

$$E(\omega) = \sqrt{S(\omega)} \exp(-i\varphi(\omega)). \quad (2.23)$$



In general the *phase*  $\phi(t)$  of the pulse is a periodic function that specifies the oscillation and its frequency of the electric field as a function of time. In case of the spectral phase  $\varphi(\omega)$ , it describes the time difference of the frequencies  $\omega$ , therefore it contains time-versus-frequency information. For a constant phase  $\varphi(\omega) = 0$  all frequencies oscillate in the same phase, which means that all have a zero crossing (in the same direction) at the same time. It is often helpful to expand the spectral phase into a TAYLOR series and analyze its components

$$\varphi(\omega) = \varphi(\omega_0) + \left. \frac{d}{d\omega} \varphi(\omega) \right|_{\omega_0} (\omega - \omega_0) + \frac{1}{2} \left. \frac{d^2}{d\omega^2} \varphi(\omega) \right|_{\omega_0} (\omega - \omega_0)^2 + \dots \quad (2.24)$$

1. The spectral phase coefficient of zeroth order is called *absolute phase* and describes the phase of the carrier wave with respect to the envelope. Since the duration of the optical cycle ( $T = c/\lambda \approx 3.4$  fs for  $\lambda = 1030$  nm) of a pulse is much shorter than the pulse duration  $\tau \approx 50$  fs considered in this thesis, the absolute phase can be assumed to have negligible influence. However, when the pulse is only a few cycles long, the absolute phase matters [2].
2. The first order term of the spectral phase corresponds to a temporal shift of the envelope in the time domain. A positive  $\varphi'(\omega_0)$  corresponds directly to a shift towards later times [11]. This can be described with the Fourier transform shift theorem which says that

$$\mathcal{F}[E(t - \tau)](\omega) = E(\omega) \exp(-i\omega\tau). \quad (2.25)$$

This time shift is called *group delay* and is defined as  $\tau_G = \varphi'(\omega_0)$ .

3. The coefficients of higher orders are the quantities that cause changes in the temporal shape of the electric field. The second derivative of the spectral phase  $\varphi''(\omega)$  is the dispersion of the group delay and often called *linear chirp*. It mainly causes an increase of the pulse duration and is defined as:

$$\text{group delay dispersion GDD} = \left. \frac{d^2}{d\omega^2} \varphi(\omega) \right|_{\omega_0}. \quad (2.26)$$

Third  $\varphi^{(3)}$  and fourth  $\varphi^{(4)}$  order coefficients cause additional distortions of the pulse. They are subsequently named third order dispersion (TOD) and fourth order dispersion (FOD). Even orders of the dispersion cause symmetrical effects on the pulse, while odd orders lead to asymmetrical distortions [2].

The name of the GDD already indicated that dispersion effects will cause second order terms to appear in the spectral phase. The reason is a dispersive medium, which causes effects such as pulse stretching. The medium can be characterized by the susceptibility  $\chi(\omega)$  to an electric field and subsequently the refractive index  $n(\omega)$ , which is connected to the magnitude  $k(\omega)$  of the wave vector via equation (2.10). Expanding the wave number  $k(\omega)$  into a TAYLOR series around the central frequency  $\omega_0$  results in

$$k(\omega) = k(\omega_0) + \left. \frac{d}{d\omega} k(\omega) \right|_{\omega_0} (\omega - \omega_0) + \frac{1}{2} \left. \frac{d^2}{d\omega^2} k(\omega) \right|_{\omega_0} (\omega - \omega_0)^2 + \dots \quad (2.27)$$

## 2.4 Spectral phase and dispersion

The derivative of the wave number with respect to frequency is closely related to a known quantity to characterize a wave packet, the

$$\text{group velocity} \quad \frac{1}{v_g} = \left. \frac{d}{d\omega} k(\omega) \right|_{\omega_0}. \quad (2.28)$$

The second derivative describes the change of the group velocity with respect to frequency and is therefore called

$$\text{group velocity dispersion} \quad \text{GVD} = \left. \frac{d^2}{d\omega^2} k(\omega) \right|_{\omega_0}. \quad (2.29)$$

It characterizes the dispersive medium and determines how the medium affects the duration of an optical pulse with the center frequency  $\omega_0$ . The group velocity dispersion (GVD) is the quantity of interest when describing the optical properties of a dispersive medium. If there are no higher order dispersion effects the pulse is called *linearly chirped*. The effects of the GVD on an optical pulse are shown in figure 2.3.

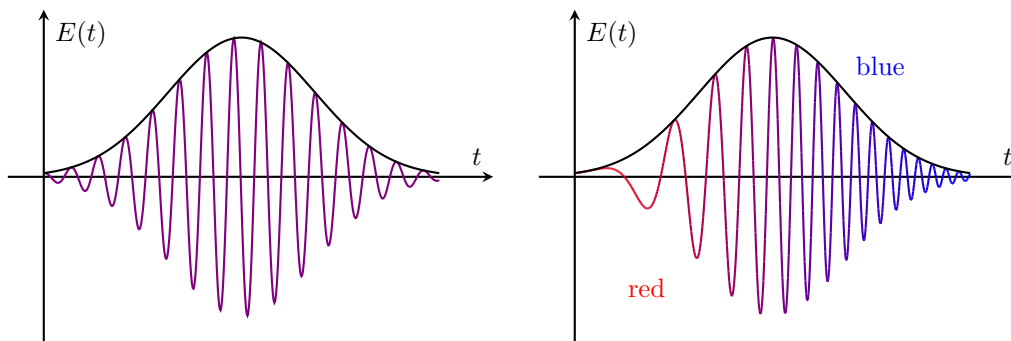


**Fig. 2.3:** Principal depiction of the amplitude of the electric field  $E(t)$  and its envelope (black) according to (2.17) without a chirped temporal phase  $\varphi(t) \propto t$  (left) and with a linearly chirped temporal phase  $\varphi(t) \propto t^2$  (right).

Travelling through a medium of length  $L$  with  $k(\omega) = n(\omega)k_0$ , the pulse accumulates phase according to  $\varphi(\omega) = k(\omega) \cdot L$ , which implies the following relation

$$\begin{aligned} \frac{d^2\varphi}{d\omega^2} &= \frac{d^2k}{d\omega^2} \cdot L \\ \Rightarrow \text{GDD}(\omega) &= \text{GVD}(\omega) \cdot L. \end{aligned} \quad (2.30)$$

To characterize the propagation of a short laser pulse, the time evolution of the GAUSSIAN envelope is considered. In a normal dispersive medium the pulse duration  $\tau$  of the GAUSSIAN pulse increases with time. This can be characterized by [12]

$$\tau(z) = \tau_0 \sqrt{1 + \left(\frac{z}{z_0}\right)^2}, \quad z_0 = \frac{\tau_0^2}{2 \cdot \text{GVD}}. \quad (2.31)$$

Since the pulse contains different frequency components the group velocities  $v_g$  differ for different frequencies. For normal dispersion ( $\text{GVD} > 0$ ) the larger (*blue*) frequencies propagate slower than the shorter (*red*) ones. This means that *red* arrives earlier at a certain value for  $z$  than *blue*, which is illustrated schematically in figure 2.4. These differences of the group velocity lead to a steady stretching of the pulse in the dispersive medium.

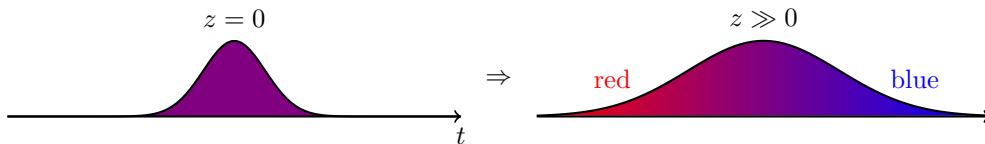


**Fig. 2.4:** Schematic representation of the pulse stretching during the propagation in a dispersive medium.

### GVD of an optical material

If an electromagnetic wave propagates through a typical dielectric medium multiple resonances occur which correspond to different lattice and electronic vibrations. The susceptibility  $\chi$  of the material arises from a superposition of contributions from these resonances [12]. Using the relation  $n^2 = 1 + \chi$ , the dependence of  $n$  on the wavelength  $\lambda$  can be approximated using the SELLMIEIER equation

$$n^2(\lambda) = 1 + \frac{B_1\lambda^2}{\lambda^2 - C_1} + \frac{B_2\lambda^2}{\lambda^2 - C_2} + \frac{B_3\lambda^2}{\lambda^2 - C_3} + \dots \quad (2.32)$$

To calculate the GVD of a material, the wave vector  $k$  is expanded into a TAYLOR series around the centre frequency  $\omega_0$  expressed as a function of the refractive index  $n$ . The wave vector  $k$  is connected to the refractive index via the dispersion relation (2.10). Using equation (2.27) it therefore follows

$$\frac{n(\omega)\omega}{c} = \frac{n(\omega_0)\omega_0}{c} + \left. \frac{d}{d\omega} \frac{n(\omega)\omega}{c} \right|_{\omega_0} (\omega - \omega_0) + \underbrace{\frac{1}{2} \left[ \frac{2n'(\omega_0) + n''(\omega_0)\omega_0}{c} \right]}_{=\text{GVD}} (\omega - \omega_0)^2 + \dots \quad (2.33)$$

A commonly used optical material is *fused silica*, for which the SELLMIEIER equation was experimentally measured in [13]. The derived coefficients are given in appendix A. Using equation (2.33) the GVD of fused silica at  $\lambda_0 = 1030$  nm can be calculated by differentiating equation (A.1) with *Mathematica* [14] which results in

$$\text{GVD}(\omega_0) = \frac{2n'(\omega_0) + n''(\omega_0)\omega_0}{c} = 18.97 \frac{\text{fs}^2}{\text{mm}}. \quad (2.34)$$

### 3. Spectral interferometry

The goal of this thesis is the characterization of the optical components of a laser amplifier. The information how a medium affects the laser pulse can be found in the refractive index  $n(\omega)$  and because of (2.10) also in the wave vector  $\mathbf{k}(\omega)$ . As already mentioned in the last section, the pulse accumulates phase according to  $\varphi(\omega) = k(\omega) \cdot L$  in a medium of length  $L$ . Therefore, the dispersion effects are contained in the spectral phase. Since the phase cannot be extracted directly from the intensity spectrum  $S(\omega)$ , an interference method is used. The spectral components of two time-shifted pulses can interfere with each other, whereby the spectral phase is imprinted on the intensity spectrum. The interferences occur as fringes in the spectrum, which is shown schematically in figure 3.1. Analyzing the spectral fringes can be used for a determination of the delay  $t_0$  and the spectral phase.

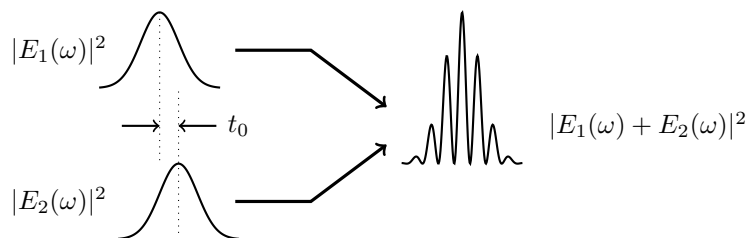


**Fig. 3.1:** Sketch of spectral interference between two laser pulses with a GAUSSIAN spectrum, one of which is delayed by  $t_0$ .

#### 3.1. The method of spectral interferometry

The method of spectral interferometry (SI) is mainly used to obtain the spectral phase difference of two GAUSSIAN pulses. In this method, two single pulses  $E_1(t)$  and  $E_2(t)$  interfere to form an interference pattern, which can be described mathematically as a superposition of two single pulses. Since the FT is linear, the spectrum  $\tilde{S}(\omega)$ <sup>1</sup> can be written as

$$\begin{aligned} \tilde{S}(\omega) &= |E_1(\omega) + E_2(\omega)|^2 \\ &\stackrel{(2.23)}{=} |\sqrt{S_1(\omega)}e^{-i\varphi_1(\omega)} + \sqrt{S_2(\omega)}e^{-i\varphi_2(\omega)}|^2 \\ &= S_1(\omega) + S_2(\omega) + 2\sqrt{S_1(\omega)S_2(\omega)} \cdot \cos(\varphi_1(\omega) - \varphi_2(\omega)). \end{aligned} \quad (3.1)$$

It is assumed that the spectral intensity of both pulses is the same  $S_1(\omega) = S_2(\omega) = S(\omega)$ . By introducing a delay  $t_0$  and using the Fourier transform shift theorem (2.25) a time delayed pulse  $E(t - t_0)$  transforms to  $E(\omega) \exp(-i\omega t_0)$ . The delay can be separated from the phase  $\varphi_1(\omega)$  and therefore the spectrum can be written as

$$\tilde{S}(\omega) \stackrel{(3.1)}{=} 2 S(\omega) [1 + \cos(\varphi_1(\omega) - \varphi_2(\omega) + \omega t_0)] \quad (3.2)$$

$$\stackrel{(2.21)}{=} 2 \cdot \exp\left(-\frac{\omega^2 \tau^2}{2}\right) [1 + \cos(\Delta\varphi(\omega) + \omega t_0)], \quad (3.3)$$

<sup>1</sup>The frequency  $\omega$  describes the shift  $\omega = \omega' - \omega_0$  to the central frequency  $\omega_0$ .

where  $\Delta\varphi(\omega) = \varphi_1(\omega) - \varphi_2(\omega)$  is the phase difference of the two GAUSSIAN pulses. The cosine indicates that depending on the delay  $t_0$  of the pulses, a periodic change in the amplitude can be observed. These spectral fringes are the key for SI. The fringe distance is inversely proportional to the delay  $t_0$ . If the number of fringes per frequency interval is counted, an estimate of the delay of the two pulses can be obtained

$$c \cdot t_0 = N_{\text{fringe}} \frac{\lambda_1 \cdot \lambda_2}{\lambda_2 - \lambda_1}, \quad t_0 = N_{\text{fringe}} \frac{2\pi}{\omega_1 - \omega_2}, \quad (3.4)$$

where  $N_{\text{fringe}}$  is the number of fringes in a given wavelength interval. An example of an interference spectrum is depicted in figure 3.2.

### Spectral phase determination

The key to characterize dispersion effects of the medium is the spectral phase, but only the intensity spectrum can be measured by a spectrometer. However, the interference spectrum can be used to retrieve the spectral phase difference  $\Delta\varphi(\omega)$  by performing an inverse FT on (3.3) into a pseudo time domain (without temporal phase information)

$$\mathcal{F}^{-1}[\tilde{S}(\omega)](t) = \frac{1}{\tau} \left( 2e^{-\frac{t^2}{2\tau^2}} + e^{-\frac{(t-t_0)^2}{2\tau^2}} e^{-i\Delta\varphi} + e^{-\frac{(t+t_0)^2}{2\tau^2}} e^{i\Delta\varphi} \right) \quad (3.5)$$

which is also depicted in figure 3.2. The FT describes which frequencies lead to the course of the measured spectrum. The spectrum contains a central peak which describes the underlying GAUSSIAN of the frequency spectrum and contains no phase information. The shifted side peaks are symmetrical and contain the spectral phase according to (3.5).

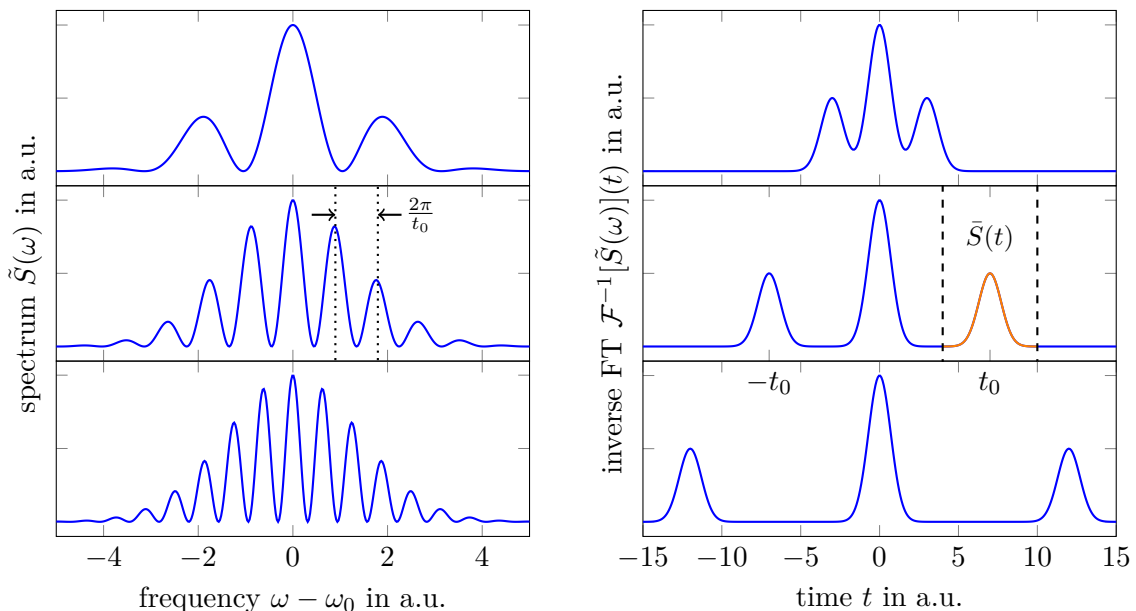


**Fig. 3.2:** The left side shows the simulated spectrum of two interfering GAUSSIAN pulses for different delays  $t_0$ . On the right the absolute value of the Fourier transform of the spectrum is depicted.

The phase can be extracted by isolating the side peak and performing a FT (2.18)

$$\begin{aligned}\bar{S}(t) &= \frac{\sqrt{2}}{\tau} e^{-\frac{(t-t_0)^2}{\tau^2}} e^{i\Delta\varphi} \\ \bar{S}(\omega) &= \mathcal{F}[\bar{S}(t)](\omega) = \exp\left(-\frac{\omega^2\tau^2}{2}\right) \exp[i(\Delta\varphi(\omega) + t_0\omega)].\end{aligned}\quad (3.6)$$

This is most commonly done by applying a window function to the FT, which is a rectangle setting all values of the spectrum outside the chosen interval to zero. The phase can be retrieved by using the general relation to acquire the phase of a complex number

$$\Delta\varphi(\omega) = -\arctan\left(\frac{\text{Im}(\bar{S}(\omega))}{\text{Re}(\bar{S}(\omega))}\right).\quad (3.7)$$

The phase  $\Delta\varphi(\omega)$  contains the information of the second order dispersion (GDD) and higher order dispersions (TOD, FOD), which can be extracted via phase differentiation.

### 3.2. GDD determination via phase differentiation

A straightforward way to determine the GDD is to differentiate the retrieved spectral phase twice according to equation (2.26). However the method of extracting the spectral phase is important for differentiation. The periodicity of the complex EULERIAN function (e.g.  $\exp(i\varphi) = \exp[i(\varphi + 2\pi n)]$  for every integer  $n$ ) causes all values of the measured phase to be initially between  $-\pi$  and  $+\pi$ . This means that infinitely many different phases correspond to the same pulse. The problem is that if the phase exceeds the value  $\pi$  it jumps back to  $-\pi$ , leaving a discontinuity. This problem is shown in figure 3.3.

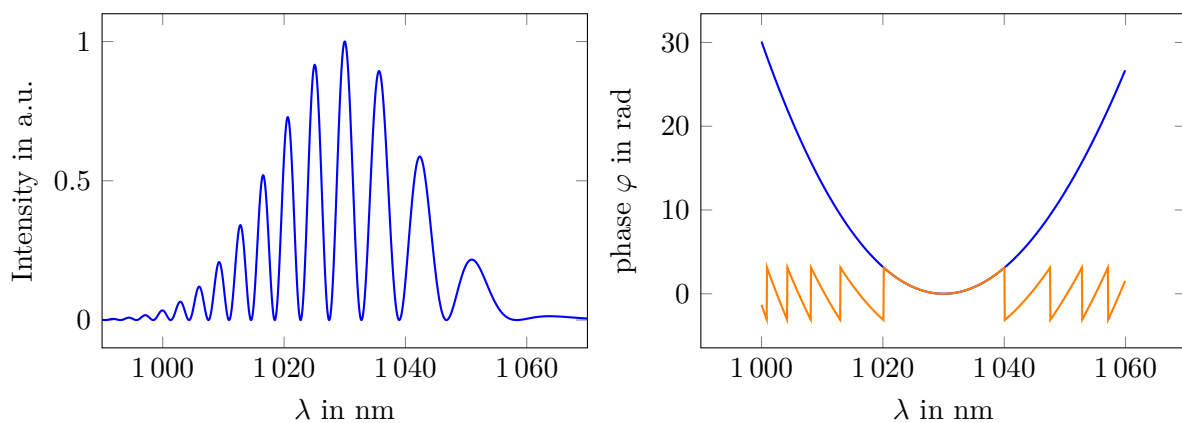


**Fig. 3.3:** A simulated spectrum of two interfering pulses with a time delay of 1 ps and a relative GDD of 10 000 fs<sup>2</sup>. The right side depicts the retrieved phase  $\Delta\varphi(\omega) - t_0\omega$  with (blue) and without (orange) phase unwrapping.

A possible solution is the *phase-unwrap*-algorithm [2]. The routine decides whether to add or subtract multiples of  $2\pi$  to preserve continuity of the measured phase. It has to be mentioned, however, that these routines only work well, if the phase difference between two sample points is smaller than  $\pi$ <sup>2</sup>.

<sup>2</sup>Consider two neighboring sample points with phases  $\varphi_1 = -\pi/2$  and  $\varphi_2 = \pi/2$ . The algorithm cannot decide, whether to add or subtract  $2\pi$ .

### Numerical differentiation method

If the resulting spectral phase can be properly unwrapped, it can be differentiated twice with respect to the angular frequency  $\omega$ . The differentiation can be implemented numerically in the following way:

$$\frac{d^2\varphi(\omega)}{d\omega^2} = \frac{d}{d\omega} \left[ \frac{d\varphi(\omega(t))}{dt} \left( \frac{d\omega}{dt} \right)^{-1} \right] = \frac{d}{dt} \left[ \frac{d\varphi(\omega(t))}{dt} \left( \frac{d\omega}{dt} \right)^{-1} \right] \left( \frac{d\omega}{dt} \right)^{-1}. \quad (3.8)$$

If the central frequency  $\omega_0$  is used here, the group delay dispersion (GDD) of the two pulses at  $\lambda_0 = 1030$  nm is obtained. However, this method requires a smooth phase and is very sensitive to noise. This will be discussed in section 4.4.3.

### Fitting method

To avoid possible influences of noise in the spectral phase, which can lead to errors during differentiation, a second approach is proposed. Thereby a high order polynomial is fitted to the spectral phase. This analytic function can be differentiated twice to retrieve the GDD. The measured phase is not only linearly chirped, which means that also higher order dispersions such as TOD and FOD occur. Therefore it is advisable to choose high order polynomial fits. The order of the fit was determined by testing different orders, checking at which order the GDD does not change anymore. A spectral phase measurement and the retrieved GDD is shown in figure 3.4.

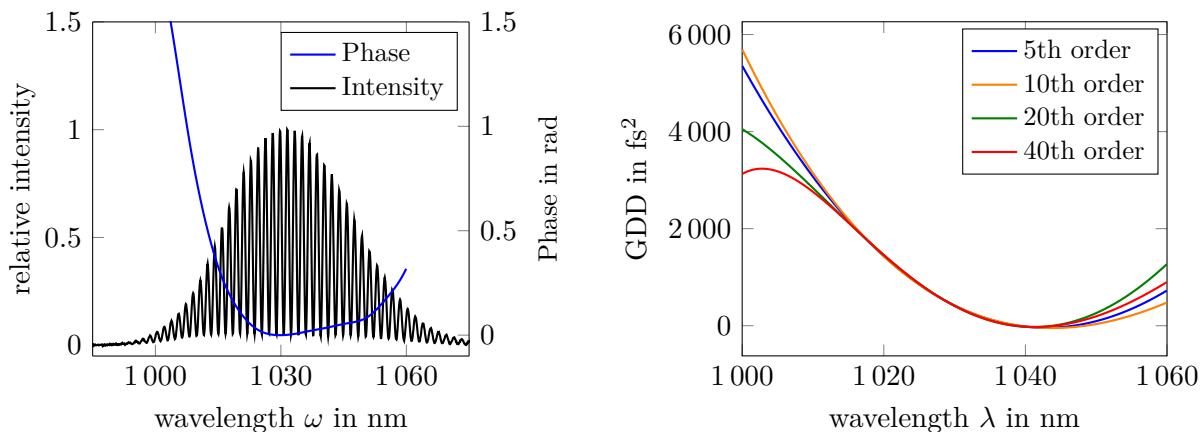


**Fig. 3.4:** Recorded measurement of the spectrum and spectral phase (without absolute phase and group delay) of two interfering pulses with a delay  $t_0 = 2$  ps. The right side shows the retrieved GDD for different orders of the polynomial fit.

It can be seen that the GDD varies a lot for different orders of polynomial fits outside the wavelength interval from 1010–1050 nm.

To characterize optical components in general, the GDD is measured with and without the optics inserted to eliminate the dispersion of the measurement setup including the mirrors, free space propagation in air and, most important, the beam splitter.

### 3.3. GDD determination via the cubic phase function

The previously discussed methods measure the group delay dispersion by taking the second-order derivative of the measured phase with respect to angular frequency obtained by a FT. The second derivative is prone to noise which is dependent on the different parameters of the phase retrieval algorithms described in section 3.2 e.g. the window width. Here, Zeng et al. developed an algorithm to determine the GDD without phase retrieval and differentiation operation [15].

The method is based on the calculation of the cubic phase function (CPF) of the FT of the interference term (3.6). Consider a cubic phase signal of a GAUSSIAN pulse shape, which can be expressed in the form of equation (2.23)

$$E(\omega) = \sqrt{S(\omega)} \exp(-i\varphi(\omega)) = \sqrt{S(\omega)} \exp[-i(\varphi_0 + \varphi_1\omega + \varphi_2\omega^2 + \varphi_3\omega^3)] \quad (3.9)$$

with  $\sqrt{S(\omega)} \stackrel{(2.21)}{=} \exp\left(-\frac{\omega^2\tau^2}{4}\right)$ .

where  $\varphi(\omega)$  is the spectral phase, expressed as a third order polynomial. It is assumed that the absolute value of the spectral phase  $\sqrt{S(\omega)}$  has a GAUSSIAN amplitude modulation. The GDD therefore is

$$\text{GDD}(\omega) \stackrel{(2.26)}{=} \frac{d^2\varphi(\omega)}{d\omega^2} = 2(\varphi_2 + 3\varphi_3\omega). \quad (3.10)$$

The cubic phase function is defined by [16]

$$\text{CPF}(\omega, T) = \int_0^\infty E(\omega + \omega')E(\omega - \omega') \exp(iT\omega'^2) d\omega'. \quad (3.11)$$

Substituting (3.9) into (3.11) yields

$$\text{CPF}(\omega, T) = S(\omega) e^{2(\varphi_0 + \varphi_1\omega + \varphi_2\omega^2 + \varphi_3\omega^3)} \int_0^\infty e^{-\frac{\omega'^2\tau^2}{2}} e^{-i[2(\varphi_2 + 3\varphi_3\omega) - T]\omega'^2} d\omega' \quad (3.12)$$

The occurring GAUSSIAN integral can be solved with the help of the known formula

$$\int_0^\infty \exp(-ax^2) dx = \frac{1}{2} \sqrt{\frac{\pi}{a}}. \quad (3.13)$$

Therefore the integral (3.12) results in

$$\text{CPF}(\omega, T) = S(\omega) e^{2\varphi(\omega)} \frac{\sqrt{\pi}}{2} \left\{ \frac{\tau^2}{2} + i[2(\varphi_2 + 3\varphi_3\omega) - T] \right\}^{-\frac{1}{2}}. \quad (3.14)$$

It can be seen that the absolute value of  $\text{CPF}(\omega, T)$  peaks along the curve  $T = 2(\varphi_2 + 3\varphi_3\omega)$ . Comparing this result with equation (3.10) shows that the peak of the cubic phase



function runs along the GDD of the spectral phase and can be used for its estimation. The GDD with respect to the angular frequency  $\omega$  can be written as

$$\text{GDD}(\omega) = \arg \max_T |\text{CPF}(\omega, T)|. \quad (3.15)$$

The numerical processing starts with an inverse FT of the equidistant spectrum. A filter is applied to extract one of the interference peaks. It is chosen such that it includes the bandwidth and excludes the noise as well [15]. The filter is realized by a program that sets all intensities outside the chosen bandwidth to zero. After that, a FT is applied. The cubic phase function can be calculated in the discrete form with the following expression [16]

$$\text{CPF}(\omega_n, T) = \sum_{m=0}^{\frac{N-1}{2}} E(\omega_{n+m}) E(\omega_{n-m}) \exp\left(-iT[m(\omega_{n+1} - \omega_n)]^2\right). \quad (3.16)$$

Here the quantity  $\Delta\omega$  is the frequency resolution of the transformed signal. The maximization is first implemented by a coarse search from 0–5000 fs<sup>2</sup> with a resolution of 5 fs<sup>2</sup> in order to get the upper and lower boundaries of the GDD. This is followed by a fine search with a resolution of the order of

$$\Delta\text{GDD} = \frac{\max(\text{GDD}) - \min(\text{GDD})}{1000}, \quad (3.17)$$

which is a resolution of 0.6 fs<sup>2</sup> for the measurement depicted in figure 3.5.

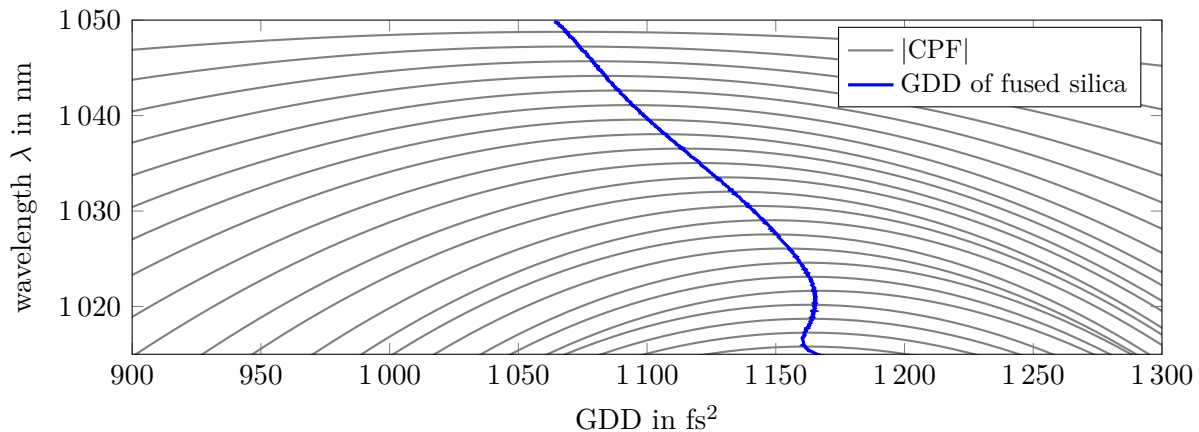


**Fig. 3.5:** To illustrate the CPF, its absolute value was calculated at 23 frequency points and normalized to the corresponding wavelength for a dispersion measurement of fused silica of length  $L = 60$  mm. It should be noted that the curvature of the CPF is shown more intensively in order to make the maximum clearer. The dispersion curve calculated from the maximization of the CPF is shown in blue.

However, it should be noted that a third order phase term with a linear chirp was used to calculate the CPF as shown in equation (3.9). This means that only constant TOD can be determined with this method. Another method for calculating higher order phase terms is proposed in [17].

## 4. Study of the spectral phase

The method of spectral interferometry (SI) will now be used to analyze different materials with known dispersion like fused silica and an Yttrium aluminium garnet (YAG) crystal. The previously introduced methods will be compared with each other and occurring experimental difficulties will be discussed. The comparison to the theoretical dispersion will lead to an estimation for which wavelength ranges the measurement can be trusted and what deviations of the resulting GDD values are acceptable.

### 4.1. Experimental setup

The system used for the measurements is a mode coupled femtosecond oscillator named *Flint FL1* with a repetition rate of  $f = (75.9 \pm 0.5)$  MHz which creates ultra short laser pulses of length  $\tau \approx 50$  fs at a centre wavelength of  $\lambda_0 = (1035 \pm 2)$  nm. The oscillator generates linear, horizontally polarized laser pulses [18].

For the spectral phase measurement via SI, a MICHELSON interferometer is utilized. Due to the use of two mirrors and only a beam splitter, the setup is very compact and offers the possibility to vary the delay. The setup is depicted in figure 4.1. A Mach-Zehnder interferometer was also discussed, but it proved to be impractical because here, the delay could not be adjusted without changing the beam path. Primarily a thin beam splitter ( $d = 3$  mm) was used for the MICHELSON interferometer. This, however, had the disadvantage that the reflexes of the front and back side of the glass could not be spatially separated. Both reflexes show a time delay and can enter the entrance of the spectrometer, which leads to an additional interference pattern, making the evaluation more difficult. Finally a thick coated glass ( $d = 9.75$  mm), which is reflective ( $(50 \pm 5)\%$ ) for an incident angle of  $45^\circ$  at 1010–1055 nm, was used as a beam splitter and spatially separated both reflexes. The fringes are detected by a spectrometer *Ocean Optics HR2000+* with a resolution of  $\delta\lambda = 0.14$  nm (FWHM) at  $\lambda_0 = 1030$  nm.

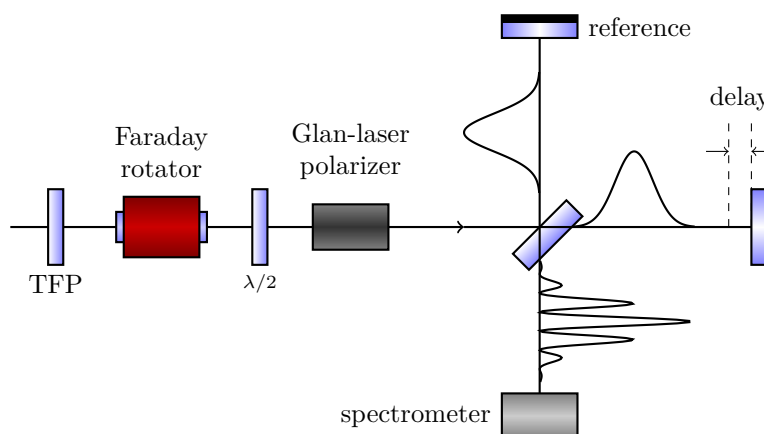


**Fig. 4.1:** Experimental setup: A MICHELSON interferometer is used to create a second pulse, which interferes with the first pulse leading to fringes in the spectral domain due to the delay between the two pulses.

A thin film polarizer (TFP) was placed in front of the MICHELSON-interferometer, which is only transmissive for p-polarized (German: “parallel”) light and reflective for s-polarized (German: “senkrecht” which means perpendicular) light. The Faraday rotator is used to ensure that the laser light returning to the input cannot return to the oscillator if the interferometer is adjusted accurately. The FARADAY rotator is based on the FARADAY effect, which describes the rotation of polarization in a medium in the presence of a magnetic field [12]. The direction of rotation depends on the orientation of the magnetic field to the direction of laser propagation. The rotator is designed in such a way that polarization direction is rotated by  $45^\circ$  when the laser passes through it once. If the propagation direction reverses, the polarization is rotated again by the same angle. Initially p-polarized light becomes s-polarized and vice versa.

## 4.2. The measurement procedure

The acquisition of the spectrum was done in LabVIEW. For that purpose a program was designed for spectral phase measurement and GDD estimation. It is described in detail in appendix C. The program shows the spectrum, calculates the spectral phase and determines the pulse delay  $t_0$  and the GDD in a wavelength range of 1010–1050 nm. At first the spectrum of the two noninterfering pulses is recorded for comparison. This is depicted in figure 4.2. When the delay of the reference is adjusted that both pulses are superimposed in space and time, they can be analyzed with spectral interferometry. Most of the measurements are conducted at a delay  $t_0 \approx 2 \text{ ps} \stackrel{\wedge}{=} 600 \mu\text{m}$ . The reason for that will be discussed in section 4.4. The performed fast Fourier transform (FFT) is also displayed in figure 4.2.

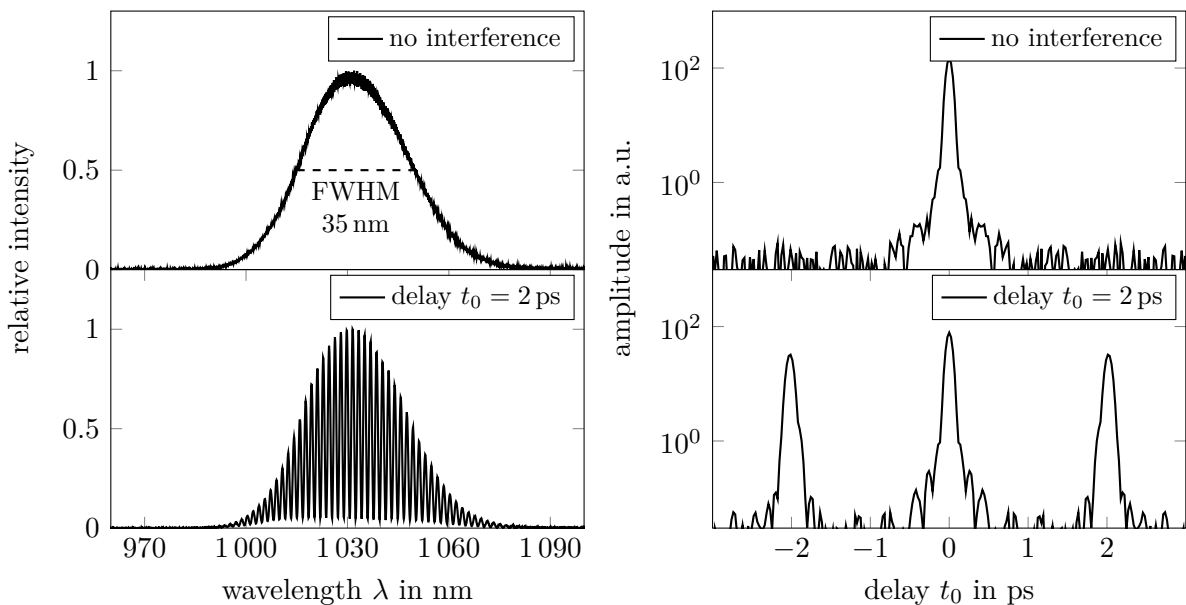


**Fig. 4.2:** Spectra of two pulses with a large delay without spectral fringes and with a delay of  $t_0 = 2 \text{ ps}$ . For the reference the FWHM was measured. The right side shows the Fourier spectrum in the pseudo time domain according to equation (3.5).

The delay  $t_0$  can be directly extracted as the difference of position of the middle peak and the shifted peaks. In figure 4.2 the magnitude of the FFT is assigned to the delay  $t_0$ , which is done by determining the time resolution of the FFT. It is given by

$$\delta t = \frac{f_{\text{sample}}}{N} = \frac{1}{\Delta\nu} = \frac{2\pi}{\Delta\omega}. \quad (4.1)$$

The expression  $f_{\text{sample}}$  denotes the sample rate and is the ratio of the number of samples  $N$  per frequency interval  $f_{\text{sample}} = N/\Delta\nu$ . The quantity  $\Delta\omega$  describes the whole frequency range of the spectrometer  $\Delta\omega = \omega_{\text{max}} - \omega_{\text{min}}$ . The time resolution  $\delta t$  describes the time step between two frequency values in the pseudo time domain. Therefore the time between two FFT values can be calculated as

$$\delta t = \frac{2\pi}{\Delta\omega} = \frac{2\pi}{(1.9737 - 1.70517) \cdot 10^{15} \text{ Hz}} = 23.39 \text{ fs}. \quad (4.2)$$

It is only used to calculate the corresponding delay  $t_0$ . The shape of the shifted peak gives no information about the actual shape of the pulse due to the lack of any phase information in the pseudo time domain.

The delay can also be estimated by using equation (3.4). 34 fringes can be counted between  $\lambda_1 = 1000 \text{ nm}$  and  $\lambda_2 = 1060 \text{ nm}$  in figure 4.2 (left), which yields a delay  $t_0 = 2.004 \text{ ps}$ . This value agrees well with figure 4.2 (right).

### 4.3. Measurement referencing with fused silica and YAG crystal

In order to assess the method of GDD determination, a measurement for a cylindrical glass of fused silica with length  $L_{\text{SiO}_2} = 30 \text{ mm}$  and a YAG crystal with  $L_{\text{YAG}} = 20 \text{ mm}$  was performed. The GDD was estimated by the phase differentiation method and via the CPF. The retrieved phases of the reference spectra (without the measurement specimen) were subtracted from the measurement spectrum before differentiating. For the CPF method the GDD for both spectra were calculated and subtracted. Dividing the GDD by the whole propagation length  $2L$  yields the GVD according to equation (2.30). Both results were compared to the theoretical curves, which were calculated using the SELLMEIER equation for fused silica (A.1) and YAG crystal (A.3) given in appendix A. The results are shown in figure 4.3.

The GVD obtained by the CPF method corresponds very well to the theoretical curves in the range of 1020–1050 nm, but outside this range occur large deviations. However, the fit method yields different results for various orders of the polynomial fit. The graph displayed in figure 4.3 shows the order with the best result for the GVD, but it can be seen that the retrieved GVD does not show the same qualitative behaviour as the theoretical curve which is nearly linear on the whole wavelength range. From the measured values it is concluded that the GDD determination of the CPF method gives correct results with an error of  $\pm 1.5\%$ . However, the absolute error is at least of the order of  $20 \text{ fs}^2$ . This value was estimated by comparing the GDD difference of several retrieved reference measurements that were recorded on different days with the same setup and calculate the deviation from zero.

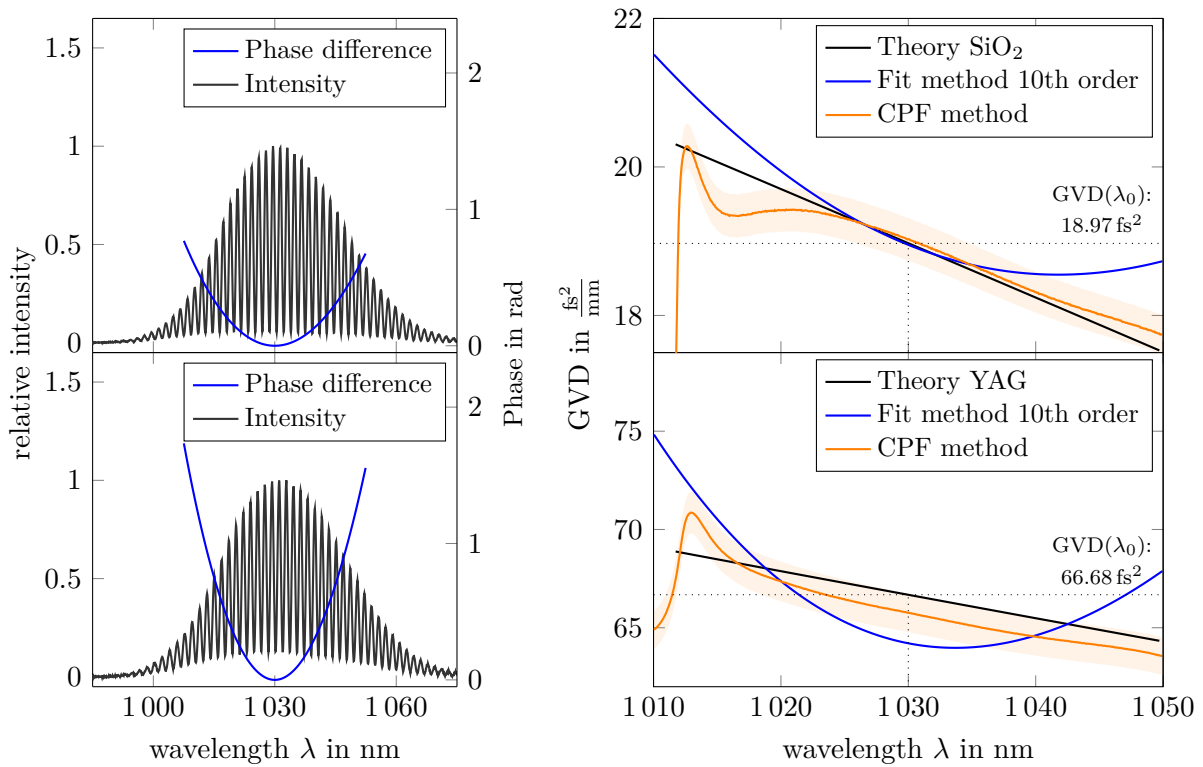


**Fig. 4.3:** Measurement of the GDD of a fused silica and YAG crystal with lengths  $L_{\text{SiO}_2} = 30 \text{ mm}$  and  $L_{\text{YAG}} = 20 \text{ mm}$  for the phase differentiation and CPF method. The intensity measurement is shown on the left, the reference measurement can be seen in figure 4.2. The depicted phase is the phase difference without the absolute phase and group delay. The shaded area represents a  $\pm 1.5\%$  deviation from the measured value. It can be seen that in this area the measured values agree with the theory. The theoretical value at  $\lambda_0 = 1030 \text{ nm}$  is indicated with a dotted line.

Despite the superiority of the measurement accuracy of the CPF method, phase differentiation offers some advantages. GDD measurements can be performed instantaneous and components can be characterized directly in LabVIEW, while the calculation of the CPF for a single measurement takes several minutes depending on the desired resolution. As figure 4.3 shows, the deviation from the theory is much greater here, so that the values can only serve as a first estimate of the GDD. As demonstrated, only values within 1020–1050 nm are valid, so from now on only this interval is shown.

#### 4.4. Experimental issues

The influences of optical media on the shape and spectral distribution of different frequencies is characterized by the GDD, which can be retrieved by SI using the previously described methods of phase differentiation and CPF. However, the determination of the GDD as second derivative of the spectral phase makes some metrological demands on the retrieval algorithm. The accurate determination of the phase is especially important, because small errors can have a strong effect on the second derivative and falsify the result.

#### 4.4.1. Spectral calibration

In order to ensure a good measurement, the first step is to calibrate the spectrometer or at least check the calibration. This was done as follows:

A calibration measurement was carried out, measuring the emission lines of vapor discharge lamps of different gases. The gases have several well characterized emission lines, which can be used for the calibration of spectrometers. Figure 4.4 shows the measured wavelength of the emission in the wavelength range between 960 nm and 1100 nm.

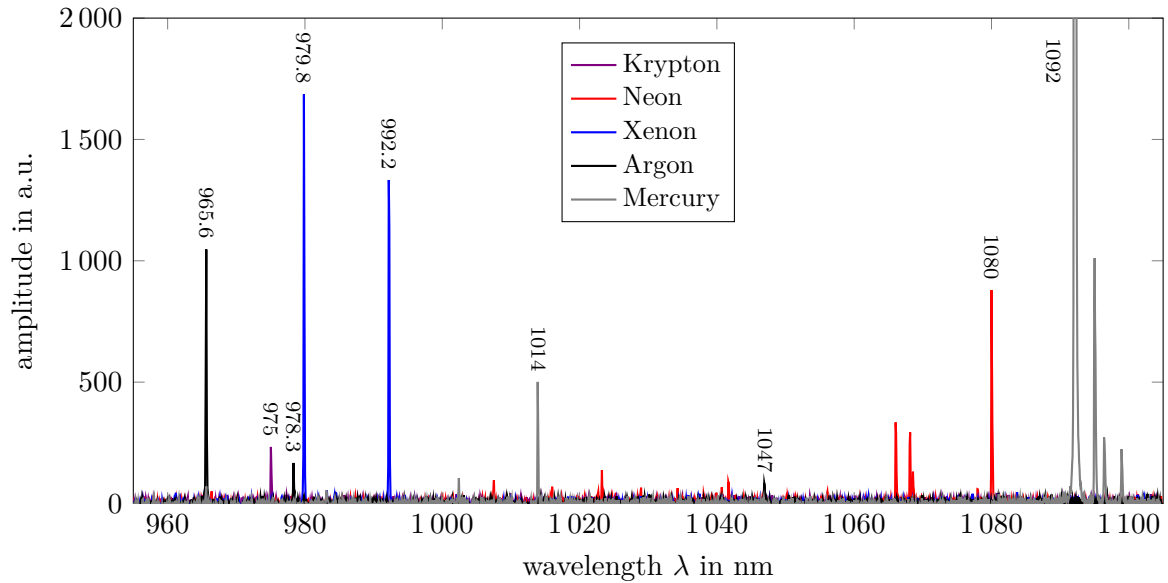


**Fig. 4.4:** Spectral lines of several elements measured with the high-resolution spectrometer *Ocean Optics HR2000+*.

The identified spectral lines of the elements were used to examine the spectral calibration of the *Ocean Optics HR2000+*. They were compared to the theoretical values of the emission, which is presented on table 4.1. It can be seen that the magnitude of the error of the calibration is of the order of 0.2 nm.

**Table 4.1:** Comparison of the measured spectral lines to the data sheet of the calibration lamps. Since the spectrometer also registers higher orders of the spectral lines, the order is also mentioned.

$\lambda$ measured [nm]	$\lambda$ [nm]	order	element
965.63	965.80	1	Argon
975.04	975.20	1	Krypton
978.34	976.00	2	Argon
979.85	980.00	1	Xenon
992.21	992.30	1	Xenon
1013.90	1014.00	1	Mercury
1080.00	1079.80	1	Neon
1092.06	1092.14	2	Mercury

In order to assess whether the measured error of the calibration has an effect on the GDD measurement, the following consideration is made according to [19]. It is assumed that the spectrometer is imperfectly calibrated and that the difference of the measured frequency  $\omega_m = 2\pi c/\lambda_m$  and the frequency  $\omega$  of the photons can be characterized by an error function:  $\omega = \omega_m + e(\omega_m)$ . According to equation (3.2) the spectrum for the phase retrieval can be written as

$$\tilde{S}(\omega) = 2S(\omega)[1 + \cos(\Delta\varphi(\omega_m + e(\omega_m)) + (\omega_m + e(\omega_m))t_0)]. \quad (4.3)$$

The spectral phase difference at the photon frequency  $\omega$  that can be retrieved is composed of two terms.

1. The first term  $\Delta\varphi(\omega_m + e(\omega_m))$  is the spectral phase difference at the shifted frequency  $\omega_m + e(\omega_m)$  and is mistaken for the spectral phase difference at  $\omega_m$ . This error is not caused by spectral interferometry and arises in many methods, which are based on spectral intensity measurements. It cannot be bypassed and should therefore be kept as small as possible [19].
2. The second term  $(\omega_m + e(\omega_m))t_0$  is a quantity which is proportional to the delay  $t_0$ . After the measured reference phase without a dispersive material is subtracted,  $e(\omega_m)$  leads to a delay dependent error [19]. Even a small calibration error can have an important effect on the retrieval of the spectral phase because it is multiplied by the delay  $t_0$ .

The paper of Dorrer [19] states that for a delay  $t_0 \approx 1$  ps and a calibration error  $\delta\lambda = 0.1$  nm (at 800 nm), the error in the phase retrieval is 0.1 rad. An easy way to correct this error is to use a reference phase. For the dispersion measurements with the MICHELSON interferometer a reference phase has to be measured anyway. Subtracting the reference phase recorded at the same delay  $t_0$  removes the spectral phase introduced by the setup, most importantly the dispersion of the beam splitter itself. It is important to keep the delay constant in order to eliminate the parasitic effects of the imperfect calibration.

There are also other possible sources of spectral errors, such as the response of the spectrometer [19] or spatial problems, such as noncollinearity of the two interfering beams due to poor adjustment of the interferometer setup or angular chirp of the beams, which influences will be discussed in section 4.4.6.

### 4.4.2. Spectral resolution

The evaluation of the spectrum is based on the characterization of the spectral fringes. In order for this to work without errors, it must be ensured that the resolution of the spectrometer is high enough. For a grating spectrometer, the spectral resolution  $\delta\lambda/\lambda = m \cdot N$  is the product of the diffraction order  $m$  and the number of grating lines  $N$ . The density of fringes in a given wavelength interval is dependent on the delay  $t_0$  between the laser pulses. This section explains which delay  $t_0$  is best suited for measuring the spectral fringes.

It is important that the correlation peak is spatially separated from the main peak, which is shown in figure 4.5.



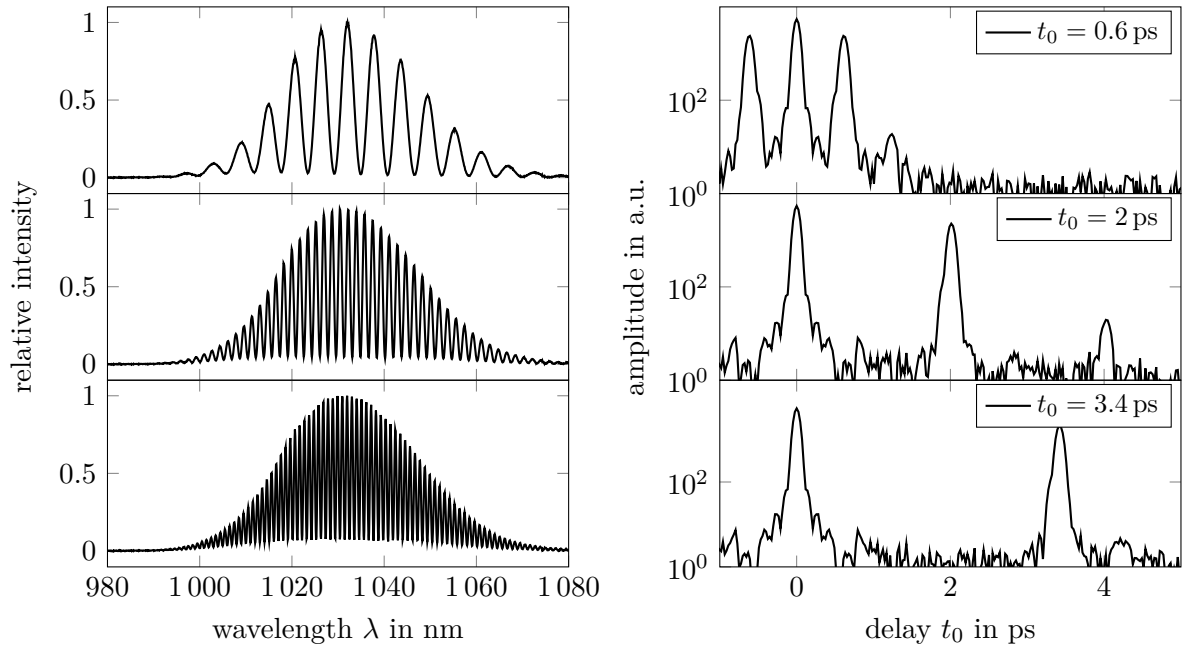


**Fig. 4.5:** Comparison of the density of fringes for different pulse delays  $t_0$ . For delays  $t_0 < 0.6$  ps the shifted peak in the Fourier spectrum merges with the central peak, which leads to errors in the phase retrieval algorithm. However, the delay must not be set too large, because then the fringes cannot be spectrally resolved anymore.

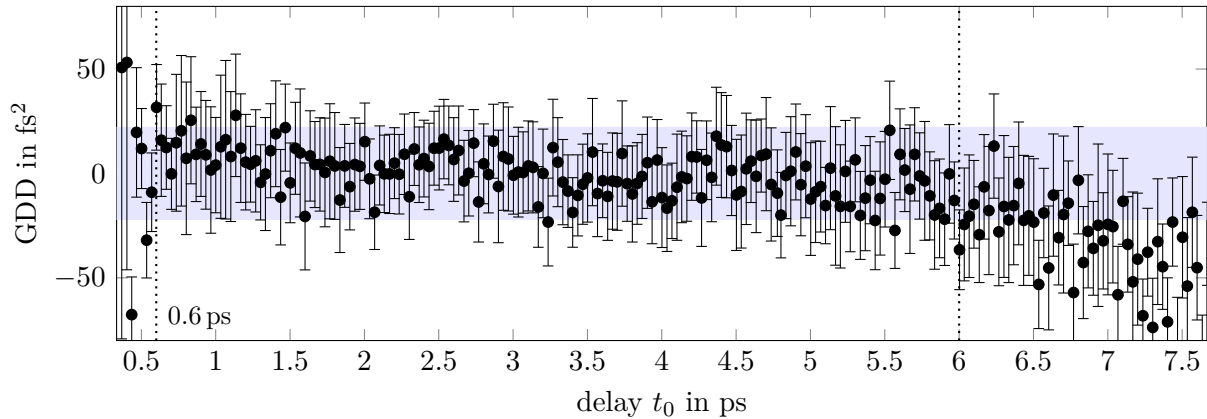
Hence the delay cannot be arbitrarily small. For this purpose an estimation of the minimum delay is needed, which can be used for an error-free measurement. Figure 4.5 shows exemplarily that for  $t_0 \geq 0.6$  ps the main and side peak in the Fourier domain can still be separated. On the other hand, larger delays lead to smaller fringe distances. In this case it must be ensured that the Fringes are spectrally sampled correctly according to the sampling theorem. Too small fringe distances also lead to a faulty measurement. It is therefore necessary to determine a delay measuring range that allows an error-free measurement of the spectral phase.

Figure 4.6 shows a measurement of the GDD difference vs. delay of two pulses for the entire possible spectral range of the spectrometer. It is expected that the GDD is not dependent on the delay, therefore all values should be in a range around a constant value. Figure 4.6 shows the doubled standard deviation of the values between 0.6–6 ps. For delays  $t_0 < 0.6$  ps and  $t_0 > 6$  ps most values are outside the standard deviation. The lower limit can be explained by the merging of the two peaks in the Fourier domain.

Additionally, a theoretical limit of the resolving power is sought. According to the NYQUIST–SHANNON sampling theorem the frequency of the fringes in the spectrum has to be smaller than two times the sampling rate. Therefore the length of one fringe period  $\delta\lambda_{\text{fringe}}$  has to be larger than two times the resolution of the spectrometer  $\delta\lambda = 0.14$  nm. According to equation (3.4) the maximum possible delay at  $\lambda_0 = 1030$  nm is

$$\begin{aligned} \delta\lambda_{\text{fringe}} &> 2\delta\lambda \\ \stackrel{(3.4)}{\Rightarrow} ct_0 &< \frac{\lambda_0(\lambda_0 + 2\delta\lambda)}{2\delta\lambda} = 3790 \mu\text{m} \triangleq 12.64 \text{ ps}. \end{aligned} \quad (4.4)$$





**Fig. 4.6:** GDD difference measurement of two pulses as a function of the delay at  $\lambda_0 = 1030$  nm. Each value is averaged over 50 individual measurements. The mean  $\overline{\text{GDD}} = 404 \text{ fs}^2$  of the values between 0.6–6 ps was subtracted from the measurement, the blue shaded area representing two times the standard deviation. The error bars represent the standard deviation of the measurements.

This value is twice as large as estimated in figure 4.6, which shows that the measurement is already influenced well before the sampling theorem is violated. For the used spectrometer, measurements must always be performed with delays in the range of 0.6–6 ps.

The mean value  $\overline{\text{GDD}}$  of the measurement in figure 4.6 can be estimated by dispersion added by the beam splitter in the interferometer. For an incident angle of  $\vartheta_1 = (45 \pm 5)^\circ$  the dispersion can be calculated using the adjacent figure 4.7. The second beam travels an extra distance  $L$  through the glass of the beam splitter. This causes a dispersion proportional to  $L$ . Using SNELL'S law with  $n_{\text{air}} \approx 1$  the refraction angle is

$$\sin \vartheta_1 = n \sin \vartheta_2 \quad \Rightarrow \quad \vartheta_2 = \arcsin \left( \frac{1}{\sqrt{2}n} \right). \quad (4.5)$$

With the thickness  $d = 9.75$  mm and the refractive index of fused silica  $n = 1.45$  at  $\lambda = 1030$  nm the length  $L$  can be calculated to

$$L = \frac{2d}{\cos \vartheta_2} \stackrel{(4.5)}{=} \frac{2d}{\sqrt{1 - \left(\frac{1}{2n^2}\right)}} = (22.3 \pm 1.8) \text{ mm}. \quad (4.6)$$

This can be used to determine the GDD via equation (2.30). With the group velocity dispersion of fused silica  $\text{GVD} = 18.97 \frac{\text{fs}^2}{\text{mm}}$  the GDD is  $(423 \pm 34) \text{ fs}^2$  which compares well with the value subtracted in figure 4.6.

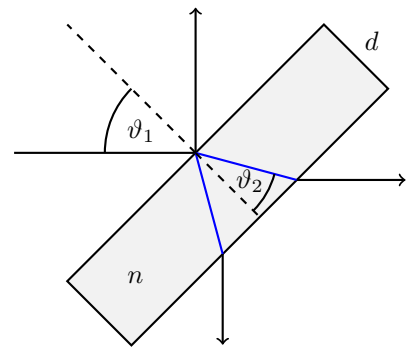


**Fig. 4.7:** Beam path in the beam splitter.

### 4.4.3. Noise sensitivity

Even for a well calibrated spectrometer, errors occur during measurements due to the inevitable noise of the spectrometer. The signal to noise ratio (SNR) plays an important role in GDD determination. Therefore, the method for which the measured GDD depends least on the noise level is searched. Achieving the highest possible SNR can be difficult because the signal at the central frequency must not saturate the spectrometer. The noise sensitivity depends on the used phase retrieval algorithm. A comparison between the numerical method and fitting method of the phase differentiation algorithm compares the GDD for different window widths in the Fourier domain. This is shown in figure 4.8.

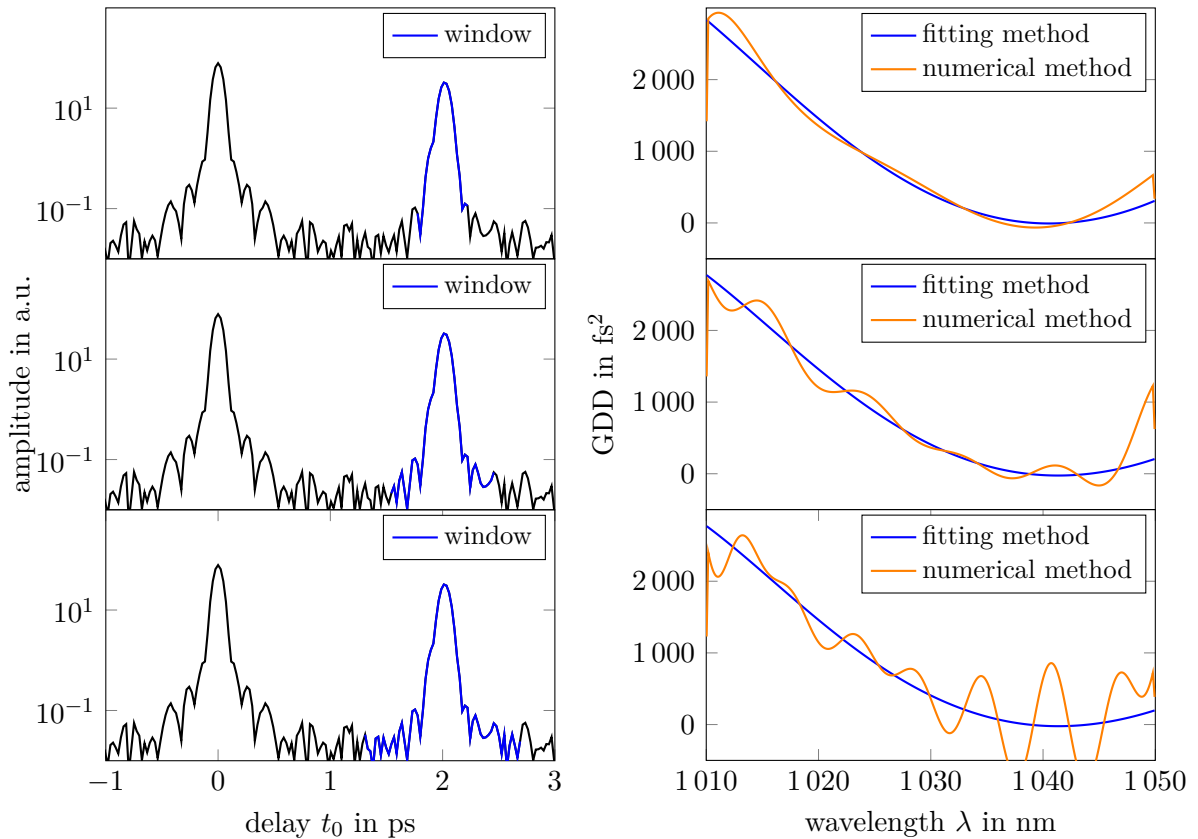


**Fig. 4.8:** Sensitivity of the retrieved GDD on the window width for different phase differentiation methods for the recorded spectrum in figure 4.2. For a large window width the noise affects the numerical retrieval algorithm and leads to large oscillations, while the fitting method is less susceptible to noise.

Figure 4.8 shows that the numerical method depends strongly on the chosen window width and therefore on the noise level. It is concluded that the method of fitting is preferable to numerical differentiation for the purpose of an online GDD estimation.

The CPF method which was proposed in section 3.3 is the least susceptible to noise because it requires no second order differentiation algorithm and can calculate the GDD directly from the FT of the pseudo time domain. For weak signals with a high noise level the CPF method is the best choice.

#### 4.4.4. Frequency sampling

One of the key aspects of SI is the Fourier transform (FT). It is done numerically via a discrete Fourier transform algorithm, commonly known as the FFT. However, this algorithm requires evenly spaced samples in the frequency domain.

The spatial coordinates  $x$  of the detector plane are equally distant and nearly proportional to the wavelength  $\lambda$  in most spectrometers [20]. This results in a nonlinear dependence of the angular frequency  $\omega$  to the wavelength array stored by the spectrometer. Because  $\omega \sim \lambda^{-1}$  the frequency steps  $\omega_{n+1} - \omega_n$  vary as much as  $\pm 37\%$  from the mean step size  $\delta\omega$  for the spectrometer *Ocean Optics HR2000+*. The maximum deviation occurs at the beginning and end of the sampling interval.

Figure 4.9 (left) shows the result of a FFT with unequal numerical sampling for different delays  $t_0$  marked by different colours. The corresponding spectra are depicted on the top of figure 4.9. The obtained array is a function of the spatial frequency  $k$  that corresponds to the FT of the spectrum  $S(x)$  as a function of the spatial coordinate [20].

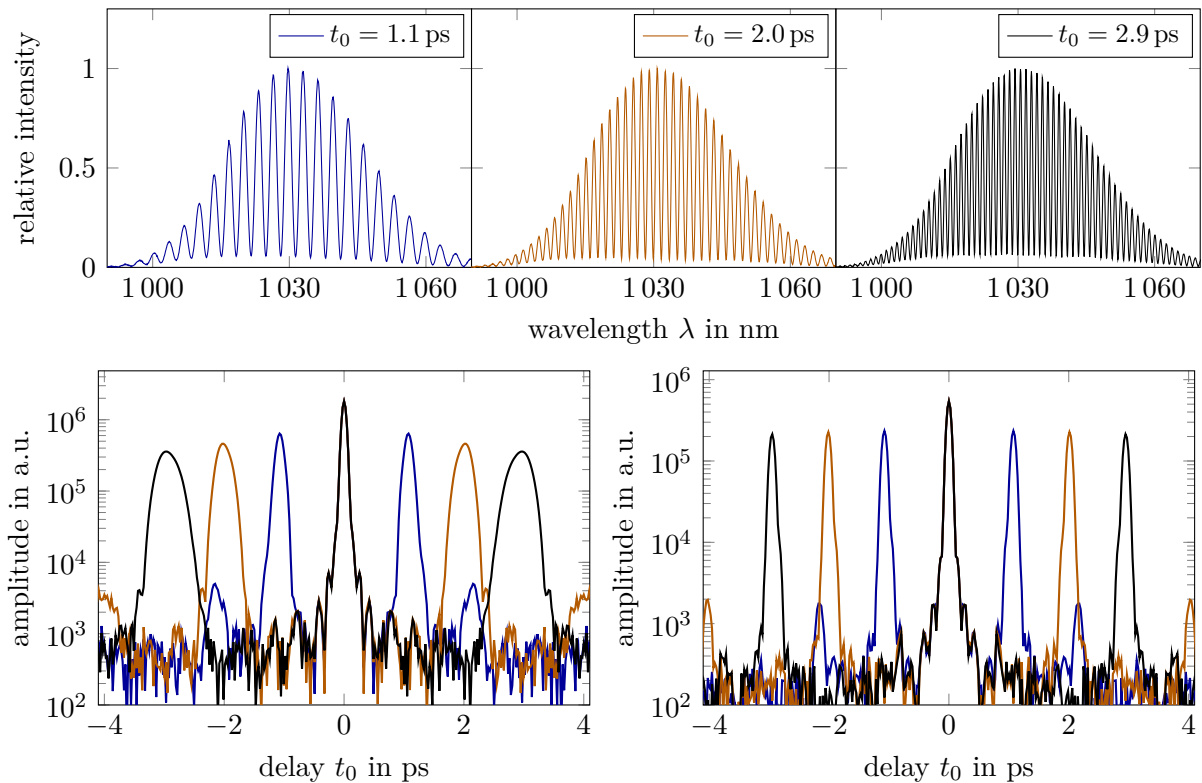


**Fig. 4.9:** The top row shows the spectrum  $\tilde{S}(\omega)$  of a reference measurement (empty interferometer) for three different delays  $t_0$ . The bottom left side shows the magnitude of the FFT of the spectra on the top, the colours are referring to the different delays  $t_0$ . The bottom right side shows the same experimental data, except that a linear interpolation of the angular frequency  $\omega$  has been performed to produce an array of evenly spaced data points.

Figure 4.9 (bottom left) shows that the correlation peak is not just simply translated in time as would be expected by (2.25), but also broadens when  $t_0$  increases. This effect was

explained by Dorrer et al. in [20].

The huge impact on the calculation of the spectral phase and thus the group delay dispersion can be shown by the derivation of the spectral phase and GDD for the spectrum of figure 4.9 with a time delay of  $t_0 = 2$  ps. The resulting GDD for two differentiation methods is depicted in figure 4.10. It shows that numerical methods fail completely in the analysis of non-interpolated spectra. A numerical evaluation of the phase obtained in figure 4.10 yields values for the GDD which oscillate between  $\pm 40\,000$  fs<sup>2</sup>. The oscillations are caused by the variations of the frequency steps and therefore its derivative, which is used in the numerical calculation (3.8).

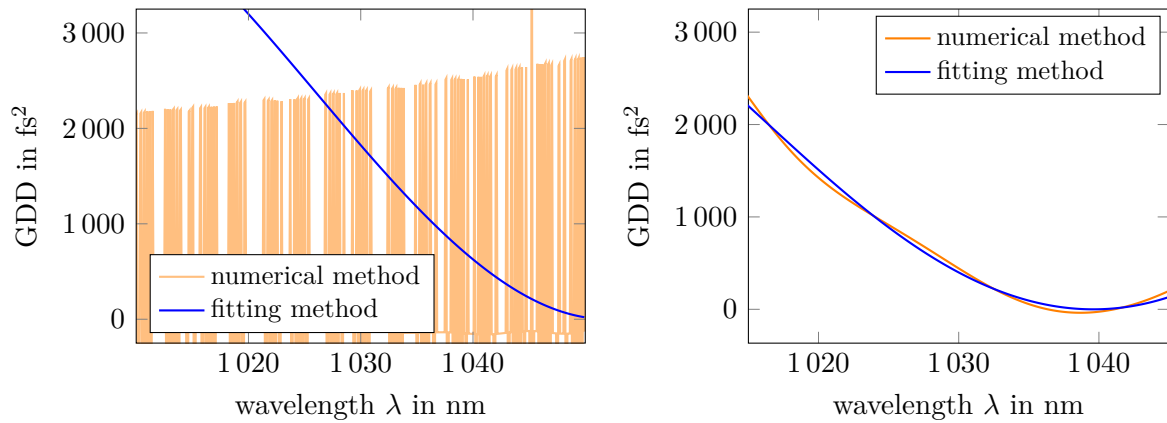


**Fig. 4.10:** The left side shows the retrieved GDD difference of two pulses for two different differentiation methods without interpolation of equidistant frequency points. The values of the numerical method were decreased by a factor of 20 for a better visualization. It can be seen that the GDD determination is not possible and the retrieval algorithm fails for numerical differentiation. The right side shows the GDD difference with interpolated data points.

One approach to solve the discrepancy discussed above is to use an algorithm that can handle nonevenly spaced data arrays. However, LabVIEW offered no function to tackle the problem this way. A straightforward solution is to first interpolate the experimental data to generate an array of evenly spaced frequencies. This was done directly in LabVIEW at the data acquisition. The change of the Fourier transform can be seen in figure 4.9 (bottom right). It was already demonstrated in figure 4.10 that the interpolation has a huge impact on the quality of any phase differentiation algorithm. The CPF function method proposed in section 3.3 also requires evenly spaced frequency points for its calculations. Therefore the interpolation was done for all measurements in this thesis.

#### 4.4.5. Change to frequency domain

The spectrum can be written in terms of the wavelength  $\tilde{S}_\lambda(\lambda)$  or frequency  $\tilde{S}_\omega(\omega)$ . The transformation between both domains is essential because the theoretical work to obtain the spectral phase involves FTs and thus frequencies, while spectrometers record the

wavelength. Using  $\omega = 2\pi c/\lambda$  the transform of the phase is

$$\varphi_\lambda(\lambda) = \varphi_\omega\left(\frac{2\pi c}{\lambda}\right). \quad (4.7)$$

For the transformation from wavelength to frequency, the law of conservation of energy must be taken into account during integration. Therefore the infinitesimal  $d\omega$  must be transformed as well so that the spectral energy remains the same in both domains [2]

$$\int_{-\infty}^{\infty} \tilde{S}_\omega(\omega) d\omega = \int_{-\infty}^{\infty} \tilde{S}_\lambda(\lambda) d\lambda = \int_{-\infty}^{\infty} \tilde{S}_\lambda\left(\frac{2\pi c}{\omega}\right) \frac{2\pi c}{\omega^2} d\omega. \quad (4.8)$$

The variable  $\lambda$  was transformed to angular frequency  $\omega$  and the infinitesimal can be expressed as  $d\lambda = -2\pi c/\omega^2 d\omega$ . This results in

$$\tilde{S}_\omega = \tilde{S}_\lambda\left(\frac{2\pi c}{\omega}\right) \frac{2\pi c}{\omega^2}. \quad (4.9)$$

This correction only has a marginal effect on the intensity  $\tilde{S}(\omega)$ , since the measured spectrum is in a narrow wavelength range of FWHM = 35 nm according to figure 4.2. In a wavelength range of 1020–1050 nm the deviation of the intensity at the edges is about  $\pm 3.5\%$ .

#### 4.4.6. Angular chirp and pulse front tilt

Up to now it has always been assumed that dispersive or diffractive effects could be treated separately. However, different optics cause a coupling between the spatial and temporal components of the electric field. This effect is utilized when stretching and compressing ultrashort pulses using prisms or gratings. The most common distortion of the pulse is the angular dispersion (AD), which is responsible that different wavelengths of the beam propagate in different directions. AD is useful because it offers the possibility of applying a negative GDD to the pulse and compressing it. However, AD also leads to another spatio-temporal distortion, the pulse front tilt (PFT). It is illustrated in figure 4.11.

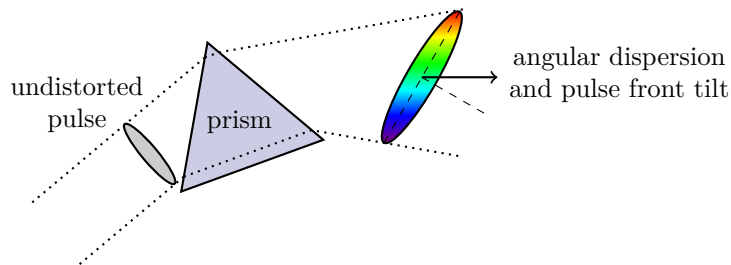


**Fig. 4.11:** Pulse front tilt caused by the angular dispersion of the prism [21].

The PFT and AD are characterized by the parameters

$$\zeta = \frac{dx_0}{d\omega}, \quad \beta = \frac{d\theta_0}{d\omega}, \quad (4.10)$$

where  $x_0$  is the center position of the  $\omega$ -component of the beam and  $\theta_0$  its propagation angle. For a GAUSSIAN spectrum with a linear chirp the evolved values of the parameters for the propagation along the  $z$ -axis are given by [21]

$$\zeta(z) = \zeta_0 + \beta z, \quad \frac{d^2\varphi}{d\omega^2} = \frac{d^2\varphi}{d\omega^2}\Big|_{z=0} - k_0\beta^2 z. \quad (4.11)$$

$\zeta(z)$  describes the increased spatial dispersion due to angular dispersion, which means that different colours in the pulse become separated from each other.  $\varphi''(z)$  describes the introduction of negative GDD due to AD, which is the basis of all pulse compressors. The effects of AD are shown in the following.

Consider a prism with an apex angle  $\gamma$ . The deviation angle  $\delta$  for a given incident angle  $\varphi_1$  is derived in appendix D and given by

$$\delta = \varphi_1 - \gamma + \arcsin \left[ \sin \gamma \sqrt{n^2 - \sin^2 \varphi_1} - \sin \varphi_1 \cos \gamma \right]. \quad (4.12)$$

The new propagation angle is therefore  $\varphi_1 + \delta$ . The angular dispersion of the prism can be written as

$$\beta = \frac{d(\varphi_1 + \delta)s}{d\omega} = \frac{d\delta}{d\omega}. \quad (4.13)$$

The second summand of  $\varphi''(z)$  in (4.11) can be interpreted as GDD, which is additionally imprinted on the spectral phase of the pulse after the prism during propagation by the length  $z$ . Figure 4.13 shows the GVD for different prisms and incident angles.

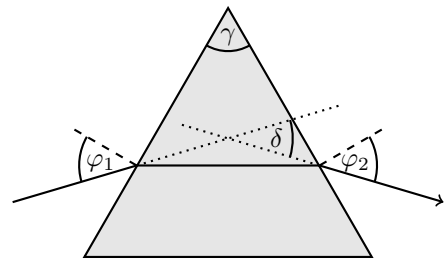


**Fig. 4.12:** Deflection angle  $\delta$  of a prism.

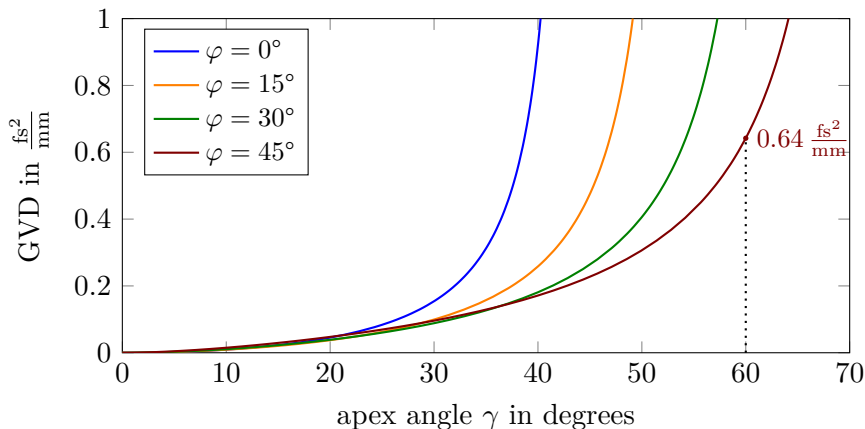


**Fig. 4.13:** The GVD =  $k_0\beta^2$  for different prism with apex angle  $\gamma$ . For a typical prism  $\gamma = 60^\circ$  the GVD for  $\varphi_1 = 45^\circ$  is  $0.64 \frac{\text{fs}^2}{\text{mm}}$ .

It turns out that the effect of AD is very small. The quantity  $z$  can be identified with the delay  $c \cdot t_0$  in the method of SI. For normal delays (see section 4.4.2)  $c \cdot t_0 \approx 0.6 \text{ mm}$  the deviation of the GDD is of the order of  $0.3 \text{ fs}^2$ , which is below the resolution of the measurement method. However, if a larger optical setup is examined by SI, where the next pulse of the oscillator is used as reference, the parameter becomes  $z = c/f_{\text{Oscillator}} \approx 3.95 \text{ m}$  and the influence of AD is no longer negligible.

## 5. Characterization of a laser amplifier

The developed methods for determining the GDD of an optical component shall now be used to characterize all components of a regenerative laser amplifier. For this purpose, each optical component is characterized individually using the method of SI and its effects on the GDD of the pulse are described.

### 5.1. Setup of the laser amplifier

The structure of the amplifier is explained in the following. The setup is shown in figure 5.1.

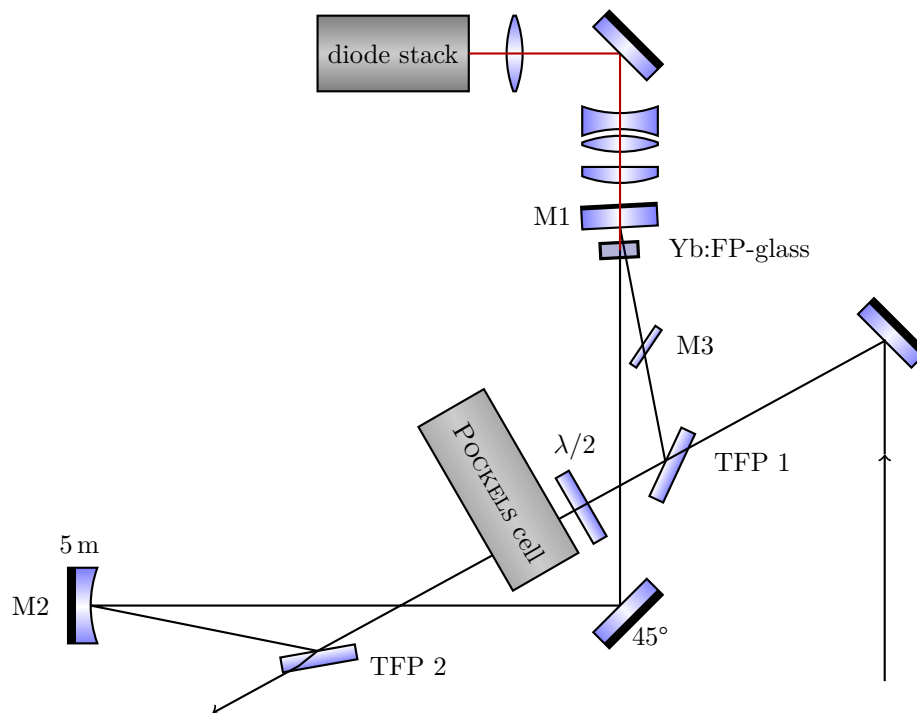


**Fig. 5.1:** Setup of the laser amplifier. The laser beam is inserted into the amplifier on the right side. The resonator consists of a concave end mirror M2 with  $R = 5$  m and a planar mirror M1 near the pump medium which is Ytterbium doped fluoride phosphate (Yb:FP) glass. The pulse is decoupled from the amplifier by a Pockels cell and a TFP. The spectral mirror M3 compensates for the unequal wavelength amplification of the active medium.

The incoming pulse is coupled into the amplifier via TFP1. The amplifier shown in figure 5.1 is designed as a regenerative ring-like cavity, where the laser pulse circulates up to 40 times during the amplification. The input and output coupling is realized by the Pockels cell. A  $\lambda/2$  plate is used to compensate the polarization rotation induced by the Pockels cell. The Ytterbium doped fluoride phosphate glass is pumped through the mirror M1, which is transmissive for the wavelength of the laser diode stack. After the amplification the pulse is decoupled at TFP2 [22].

## 5.2. Characterization of the optical components

For a complete description of the laser amplifier the optical components are individually characterized. As already shown in section 4, the CPF method provides the most accurate results in determining the GDD with an accuracy of  $\pm 1.5\%$  within the spectral range of 1020–1050 nm. The following components are therefore analyzed with this method. For the measurement, the spectral phase is recorded using SI and compared to a reference spectrum. The relative phase is displayed, whereby the absolute phase value  $\varphi_0$  and the group delay  $\tau(\omega) = \varphi'(\omega_0)(\omega - \omega_0)$  are subtracted since they have no physical significance (see section 2.4). In the measurement of several components, the pulse passes the optical component twice. For these cases, the values obtained were halved in order to characterize all components for a single resonator cycle.

### Short pass filter (pump mirror)

The first component to characterize is a short pass filter M1 of figure 5.1, which is transmissive for the light of the diode stack and reflective for the pulse in the amplifier. Three possible filters, which can be used as pump mirrors M1 in the amplifier, with different transmission ranges were measured. The measurement was performed by exchanging one mirror of the MICHELSON-interferometer with a short pass filter and comparing the GDD to the measurement of a silver mirror.

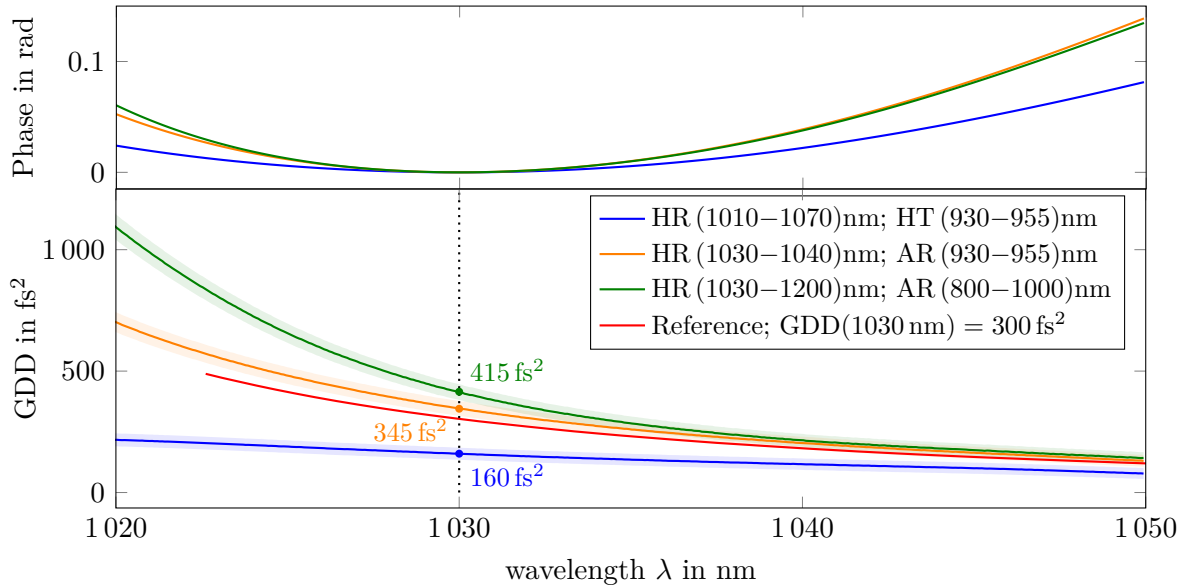


**Fig. 5.2:** Phase (top) and GDD measurement (bottom) of three different short pass filters which are high reflective (HR), high transmissive (HT) or anti reflective (AR) in certain wavelength ranges. The reference refers to a digitized GDD calculation of the manufacturer *Layertech* GmbH of the second short pass filter (orange). Errors can also occur in the reference because it was theoretically calculated by the manufacturer.

It can be seen in figure 5.2 that the reference curve deviates from the measurement of the second short pass filter (orange) by about 10 %, but the qualitative behaviour is the same. This can be due to errors in the digitization process or calculation errors of the



reference itself. It can be seen that the GDD is nearly constant for larger wavelengths, where the filters are highly reflective. However, for wavelengths smaller than 1030 nm the GDD increases to large values.

### Laser and 45° mirror, active medium and Pockels cell

The next component to characterize is the end mirror of the resonator with a radius of curvature  $R = 5$  m. It is highly reflective for an incident angle of  $0^\circ$  in a wavelength range between 1030–1084 nm. The other components are the Yb:FP glass, which is the active medium, a deflection mirror which is highly reflective at an incident angle of  $45^\circ$  in a wavelength range between 970–1070 nm and the Pockels cell. The spectral phase difference and the GDD of all four components are compared in figure 5.3. The mirrors were measured in reflection, while the Pockels cell and Yb:FP glass were analyzed by inserting them into the beam path of the interferometer. The values (except for the end mirror) were halved as mentioned before.

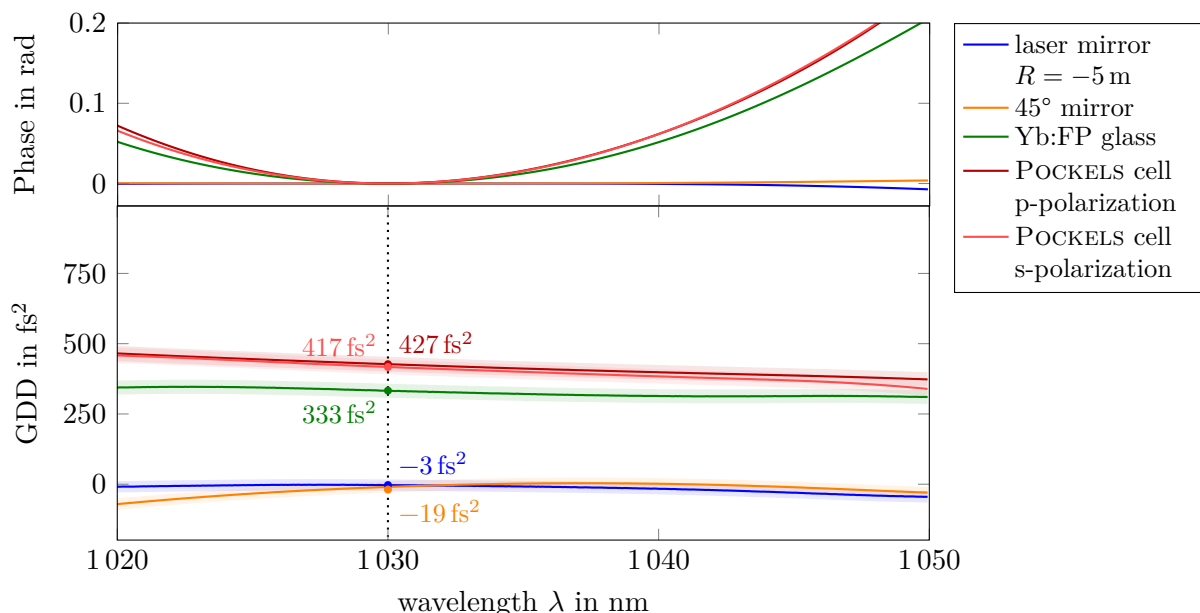


**Fig. 5.3:** Phase difference (top) and GDD measurement (bottom) of a curved laser mirror with  $R = 5$  m, a  $45^\circ$  deflection mirror, the Yb:FP glass and the Pockels cell in p-polarization and s-polarization.

Figure 5.3 shows that the laser mirror and the  $45^\circ$  deflection mirror imprint hardly any significant GDD onto the pulse. Their values for the GDD at  $\lambda = 1030$  nm are within the error tolerance range for a constant GDD of  $0$   $\text{fs}^2$ . However, the Yb:FP glass imprints a GDD of  $333$   $\text{fs}^2$  with no significant change along the wavelength range. The Pockels cell adds a GDD of about  $420$   $\text{fs}^2$  to the pulse regardless of the polarization. This value has to be compared to the theoretical dispersion of the crystal in the Pockels cell, potassium dideuterium phosphate (KD\*P) [23], which has a GVD at 1030 nm of  $14.63 \frac{\text{fs}^2}{\text{mm}}$  (see appendix A). For a crystal length of 2 cm, the corresponding GDD is  $293$   $\text{fs}^2$ . This is lower than the measured dispersion, because the hygroscopic material is additionally covered by two windows of fused silica.

### TFP, spectral mirror and half wave plate

The last components to analyze are the two TFPs of the amplifier setup and additionally a spectral mirror with a GAUSSIAN reflexion profile for s-polarized light. The characteristics of the TFP and spectral mirror were measured for p-polarized and s-polarized light. The TFP is transmissive for p-polarized light and reflective for s-polarized light at an incident angle of  $65^\circ$ . Therefore, the measurement setup was slightly altered as depicted in figure 5.4. The spectral mirror was measured in transmission at an angle of  $45^\circ$ . The measurement of the spectral phase difference and GDD is shown in figure 5.5.

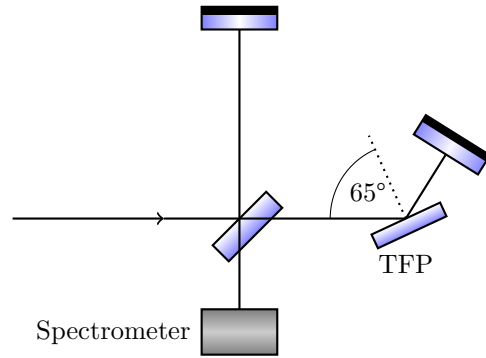


**Fig. 5.4:** Setup for the GDD measurement of the TFP (s-polarization).

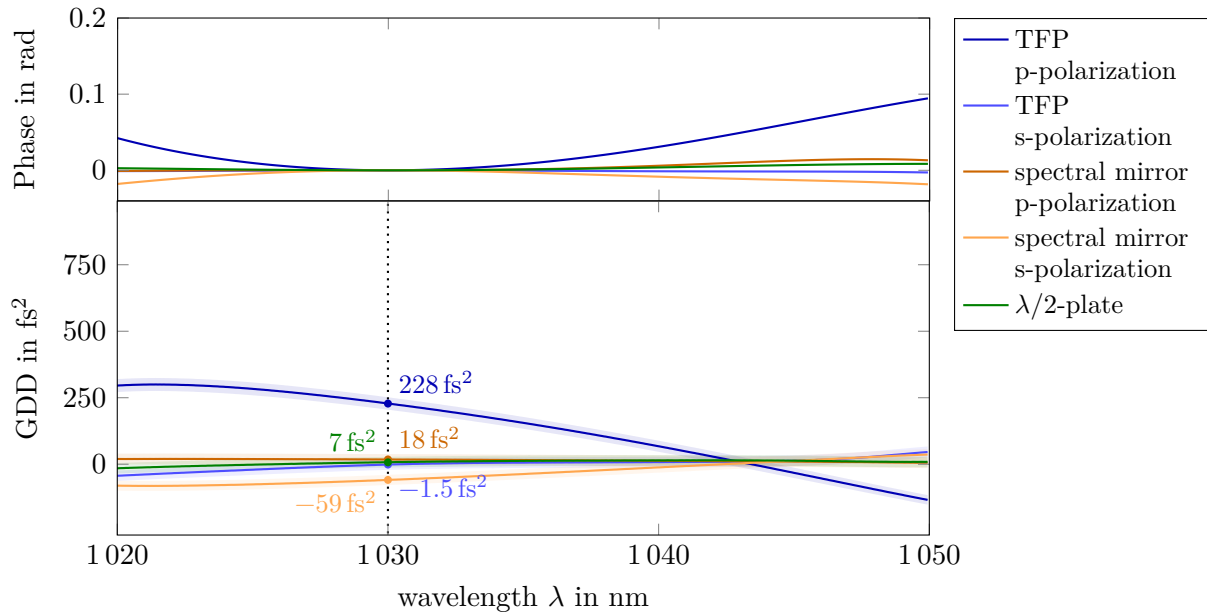


**Fig. 5.5:** GDD measurement of a TFP, spectral mirror FP15 with a Gaussian reflexion profile in p-polarization and s-polarization and a  $\lambda/2$ -half wave plate.

It turns out that the influence of the TFP in the case of reflexion (s-polarization) is very small, the same applies to the transmission of the  $\lambda/2$  half wave plate. In the case of transmission of the TFP, a larger GDD is observed. This may be explained by the pulse travelling through the material of the TFP with a thickness  $d = 8$  mm. The result is compared with a plate of fused silica of the same thickness  $d = 8$  mm and an incident angle of  $65^\circ$ . Modifying equation (4.6), this results in a value of  $194$  fs<sup>2</sup>, which is similar to the effect of the TFP. It is therefore assumed that the dispersive effect of TFP is mainly caused by the material and not by the polarizing layer. The influence of the spectral mirror for s-polarized light is smaller, but can be distinguished from the reference measurement with p-polarized light.

### Phase dispersion after a whole resonator cycle

To characterize the entire resonator of the amplifier, the spectral phase and the GDD of the individual components of the amplifier are summed up. According to figure 5.1 the optical components interacting with the beam in one resonator cycle are two TFPs, a half wave plate, the POCCKELS cell, the end mirror, the pump mirror (second short pass filter) and the active medium (Yb:FP-glass) twice. The summation for GDD and spectral phase is shown in figure 5.6.

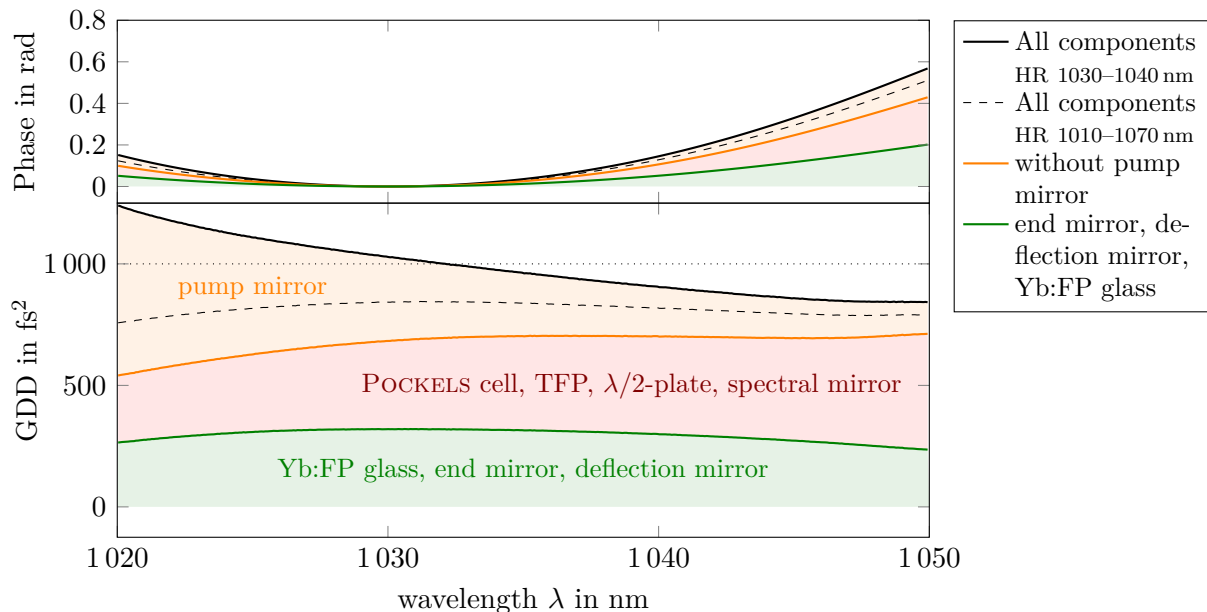


**Fig. 5.6:** Summation of the spectral phase difference (top) and GDD (bottom) of all components (with pump mirror HR 1030–1040 nm) of the laser amplifier for a single cycle. The dashed line indicates the summation with another pump mirror with a larger reflection window. The individual shares to the total value (black) are indicated by the shaded areas. It can be seen that the major influences on the GDD of the pulse are the pump mirror and the POCCKELS cell.

Most of the dispersion during a cycle in the resonator is caused by the short pass filter and the POCCKELS cell. The green shaded area shown in figure 5.6 is mainly caused by the Yb:FP glass. The total group velocity dispersion is  $(1000 \pm 150) \text{ fs}^2$  averaged over the whole wavelength range. At 1030 nm the value is  $1080 \text{ fs}^2$ .

The retrieved averaged GDD can be used to estimate the length of a 50 fs pulse after one cycle in the amplifier. According to equation (2.31), the pulse length can be calculated to

$$\tau = \tau_0 \sqrt{1 + \left( \frac{2 \cdot \text{GDD}}{\tau_0^2} \right)} = 64 \text{ fs}, \quad (5.1)$$

which is an increase of 28 %.

### Phase dispersion after the amplification

During the amplification the laser pulse circulates up to 40 times. The whole dispersion of the amplifier can be determined by adding the effects of 40 resonator cycles to the dispersion effects of the TFP on p-polarized light during input and output coupling. The spectral phase and GDD are presented in figure 5.7.

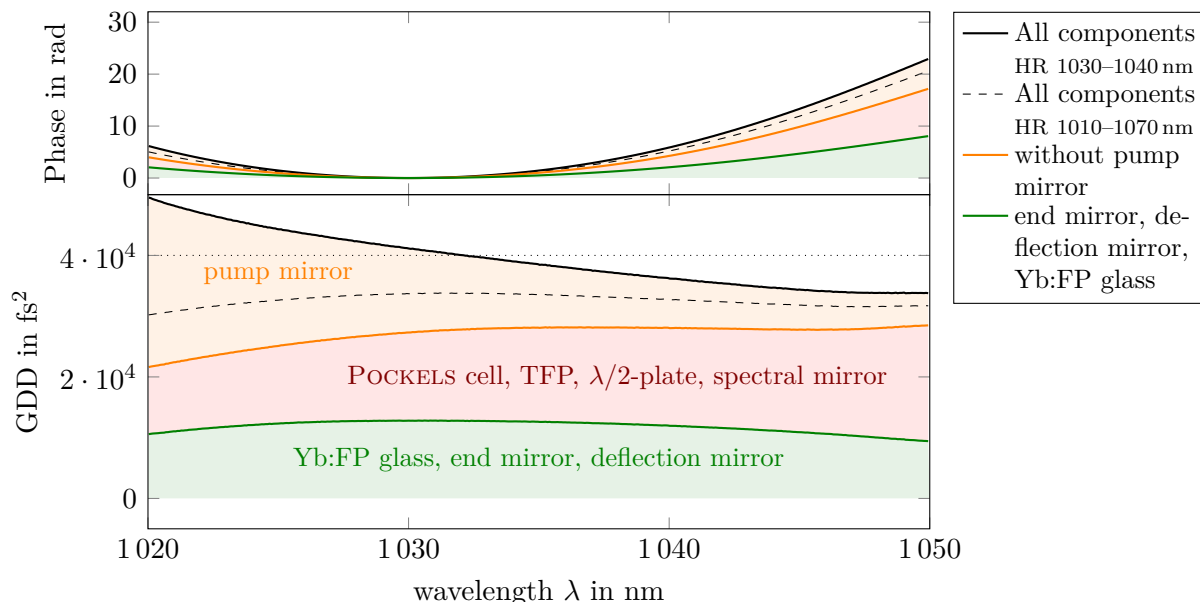


**Fig. 5.7:** Summation of the spectral phase difference (top) and GDD (bottom) of all components (with pump mirror HR 1030–1040 nm) of the laser amplifier for the whole amplification (40 resonator cycles, input and output coupling). The dashed line indicates the summation with another pump mirror with a larger reflection window. The individual shares to the total value (black) are indicated by the shaded areas.

It turns out that the additional dispersion caused by the coupling and decoupling of the pulse is negligible compared to the total dispersion. Compared to figure 5.6, the qualitative course of the GDD does not change. It results in an averaged value of  $40\,000\text{ fs}^2$  over the whole wavelength range. For the whole amplification process the stretching of a 50 fs pulse can be calculated as well. Analogous to equation (5.1) the pulse length can be calculated to  $\tau = 1.6\text{ ps}$ .

## 6. Conclusion

Spectral interferometry (SI) is a promising method to characterize the dispersion of a medium and its effects on a laser pulse. It is a reliable technique for measuring the spectral phase, which is important for analyzing effects such as stretching of the pulse duration and changes of the temporal shape. This Bachelor thesis dealt with a detailed derivation and introduction of SI. It was presented how the phase difference of two pulses can be derived by using Fourier transform (FT) and which assumptions have to be made. For the evaluation of the spectral phase and the determination of the second derivative, the group delay dispersion (GDD), different procedures were introduced and compared. In the first method the measured spectral phase is directly differentiated twice with respect to the angular frequency. This was done either numerically or by taking the second derivative of a high order polynomial fit of the retrieved spectral phase. Since this method is very susceptible to small disturbances of the spectral phase, a second method was searched for, in order to obtain the GDD directly. For this purpose the cubic phase function (CPF) was introduced, the maximum of which can be used to determine the GDD. It turned out that the method of the CPF gives more accurate results. Measurements of fused silica and YAG crystal showed that the retrieved GDD describes the theoretical values with a deviation of  $\pm 1.5\%$  in a wavelength range of 1020–1050 nm. The small wavelength range results from the fact that the CPF method requires a high SNR of the spectrum to work properly. The algorithm for calculation and maximization of the CPF is time consuming. Depending on the desired resolution, the algorithm takes several minutes for an evaluation of a single measurement. The differentiation method, however, offers the advantage that the data evaluation can be performed instantaneous at the time of data acquisition, which is advantageous for quick GDD measurements. For the measurement of the spectral phase a LabVIEW application was developed, which automatically reads the data of the spectrum and calculates the spectral phase and all phase orders with the phase differentiation method up to the third order dispersion (TOD).

When measuring the spectral phase, possible sources of errors must be excluded. This means that the spectrometer should be calibrated as accurately as possible. Since the calibration errors depend on the delay  $t_0$  between the pulses, they can be minimized by recording the measurement for a certain optical element and the reference at the same delay of both pulses. Furthermore, the delay should be selected to match the resolution of the spectrometer. For the measurement with the spectrometer used in this thesis, a possible measurement range for  $t_0 = 0.6\text{--}6\text{ ps}$  was found. For values below the range, errors are caused by the merging of the main peak with the side peak in the Fourier domain, whereas values above the determined range violate the sampling theorem for the resolution of the spectral fringes. For the inverse FT of the pseudo time domain back into the frequency domain a suitable window should always be selected. This window should contain the complete shifted peak and additionally exclude the main peak and as much noise as possible. Furthermore, when using a FFT, it is important to use an equidistantly sampled spectrum in the frequency domain, which can be achieved by interpolating the spectrum. For both the phase differentiation method and the CPF method, the signal to noise ratio (SNR) should be as large as possible when recording the spectra. Other effects like angular dispersion (AD) cause only small changes in GDD, which are below

the measurement accuracy of the methods used in this thesis.

A laser amplifier system with a ring-shaped resonator was constructed and the individual components were characterized with the help of SI. The spectral phase and the GDD of each component were recorded and the effects of the individual optics on the pulse length were discussed. It was found that the resonator mirror, the  $45^\circ$  deflection mirror, the TFP in reflection with s-polarized light have a negligible effect on the relevant phase terms. The material of the Pockels cell produces a large dispersion in both polarization directions, the short pass filter and the Yb:FP glass both provide an additional GDD on the pulse. A single cycle in the resonator causes the pulse to be stretched by 28%. After many resonator cycles, the accumulated dispersion is on average  $40\,000\text{ fs}^2$  in a wavelength range between 1020–1050 nm and can cause a significant change in the temporal shape, stretching a 50 fs pulse to 1.6 ps.

The amplifier setup should have the least possible influence on the GDD of the pulse. It is therefore important to select the components with the major influences carefully. Since the pump mirror has a large impact on the GDD of the laser pulse, mirrors with a flat dispersion profile should be preferred. Generally these are short pass filters whose reflection edge is far from the central wavelength, however, the filter should still be highly transmissive for the light of the diode stack. The method of SI can therefore be used to determine the dispersion profile of the short pass filter and help to decide which is best suited as the pump mirror of the amplifier. Furthermore, by determining the pulse length behind the amplifier, it is possible to calculate an adjustment for the setup of the compressor in order to obtain the desired pulse length. SI can be used to further investigate other influences of any optical component of the CPA system on the pulse.

## References

- [1] D. Strickland and G. Mourou, "Compression of amplified chirped optical pulses," *Optics communications*, vol. 56, no. 3, pp. 219–221, 1985.
- [2] R. Trebino, *Frequency-resolved optical gating: the measurement of ultrashort laser pulses*. Springer Science & Business Media, 2012.
- [3] C. Froehly, A. Lacourt, and J. C. Vienot, "Time impulse response and time frequency response of optical pupils.: Experimental confirmations and applications," *Nouvelle Revue d'Optique*, vol. 4, no. 4, p. 183, 1973.
- [4] E. Tokunaga, A. Terasaki, and T. Kobayashi, "Femtosecond phase spectroscopy by use of frequency-domain interference," *J. Opt. Soc. Am. B*, vol. 12, pp. 753–771, May 1995.
- [5] J. P. Geindre, P. Audebert, A. Rousse, F. Fallières, J. C. Gauthier, A. Mysyrowicz, A. D. Santos, G. Hamoniaux, and A. Antonetti, "Frequency-domain interferometer for measuring the phase and amplitude of a femtosecond pulse probing a laser-produced plasma," *Opt. Lett.*, vol. 19, pp. 1997–1999, Dec 1994.
- [6] L. Lepetit and M. Joffre, "Two-dimensional nonlinear optics using fourier-transform spectral interferometry," *Opt. Lett.*, vol. 21, pp. 564–566, Apr 1996.
- [7] L. Zheng, O. A. Konoplev, and D. D. Meyerhofer, "Determination of the optical-axis orientation of a uniaxial crystal by frequency-domain interferometry," *Opt. Lett.*, vol. 22, pp. 931–933, Jun 1997.
- [8] C. Iaconis and I. A. Walmsley, "Spectral phase interferometry for direct electric-field reconstruction of ultrashort optical pulses," *Opt. Lett.*, vol. 23, pp. 792–794, May 1998.
- [9] A. Weiner, *Ultrafast optics*, vol. 72. John Wiley & Sons, 2011.
- [10] T. Pertsch, *Vorlesungsskript Grundkonzepte der Optik*. Friedrich-Schiller-Universität Jena, 2014.
- [11] F. Träger, *Springer handbook of lasers and optics*. Springer Science & Business Media, 2012.
- [12] B. E. Saleh and M. C. Teich, *Fundamentals of Photonics*. Wiley, 2019.
- [13] I. H. Malitson, "Interspecimen comparison of the refractive index of fused silica," *Josa*, vol. 55, no. 10, pp. 1205–1209, 1965.
- [14] W. R. Inc., "Mathematica, Version 12.1." Champaign, IL, 2020.
- [15] C. Zeng, H. Zhang, D. Jia, T. Liu, and Y. Zhang, "Group delay dispersion measurement from a spectral interferogram based on the cubic phase function," *IEEE Photonics Journal*, vol. 6, no. 6, pp. 1–9, 2014.
- [16] P. O'Shea, "A new technique for instantaneous frequency rate estimation," *IEEE Signal Processing Letters*, vol. 9, no. 8, pp. 251–252, 2002.

- [17] R. Cao, M. Li, L. Zuo, Z. Wang, and Y. Lu, “A new method for parameter estimation of high-order polynomial-phase signals,” *Signal Processing*, vol. 142, pp. 212–222, 2018.
- [18] Light Conversion, UAB, *Factory test certificate of FLINT femtosecond oscillator*, 2019.
- [19] C. Dorrer, “Influence of the calibration of the detector on spectral interferometry,” *JOSA B*, vol. 16, no. 7, pp. 1160–1168, 1999.
- [20] C. Dorrer, N. Belabas, J.-P. Likforman, and M. Joffre, “Spectral resolution and sampling issues in fourier-transform spectral interferometry,” *JOSA B*, vol. 17, no. 10, pp. 1795–1802, 2000.
- [21] S. Akturk, X. Gu, E. Zeek, and R. Trebino, “Pulse-front tilt caused by spatial and temporal chirp,” *Optics express*, vol. 12, no. 19, pp. 4399–4410, 2004.
- [22] H. Liebetrau, *Erzeugung und zeitliche Streckung kontrast-optimierter Seed-Pulse für Hochintensitätslaser bei 1030 nm*. PhD thesis, 2017.
- [23] K. W. Kirby and L. G. DeShazer, “Refractive indices of 14 nonlinear crystals isomorphic to  $\text{kh}_2\text{po}_4$ ,” *J. Opt. Soc. Am. B*, vol. 4, pp. 1072–1078, Jul 1987.
- [24] D. E. Zelmon, D. L. Small, and R. Page, “Refractive-index measurements of undoped yttrium aluminum garnet from 0.4 to 5.0  $\mu\text{m}$ ,” *Appl. Opt.*, vol. 37, pp. 4933–4935, Jul 1998.
- [25] M. Bass, E. Van Stryland, D. Williams, and W. Wolfe, *Handbook of optics, Volume II: Devices, Measurements, and Properties*. McGraw-Hill, Inc., 1995.



## 7. List of abbreviations

<b>AD</b>	angular dispersion
<b>CPA</b>	chirped pulse amplification
<b>CPF</b>	cubic phase function
<b>FFT</b>	fast Fourier transform
<b>FT</b>	Fourier transform
<b>FOD</b>	fourth order dispersion
<b>FROG</b>	frequency resolved optical gating
<b>FWHM</b>	full width at half maximum
<b>GDD</b>	group delay dispersion
<b>GVD</b>	group velocity dispersion
<b>LabVIEW</b>	Laboratory Virtual Instrumentation Engineering Workbench
<b>laser</b>	light amplification by stimulated emission of radiation
<b>PFT</b>	pulse front tilt
<b>POLARIS</b>	Petawatt Optical Laser Amplifier for Radiation Intensive Experiments
<b>SI</b>	spectral interferometry
<b>SNR</b>	signal to noise ratio
<b>SPIDER</b>	spectral phase interferometry for direct electric field construction
<b>TFP</b>	thin film polarizer
<b>TOD</b>	third order dispersion
<b>VI</b>	visual instrument
<b>YAG</b>	Yttrium aluminium garnet
<b>Yb:FP</b>	Ytterbium doped fluoride phosphate

## A. Sellmeier equations of the used materials

In order to evaluate the experimental results of a GDD measurement, the theoretical GVD of the material should be known. The most commonly used material is fused silica, which SELLMEIER coefficients were estimated by [13]. The dispersion formula can be written as

$$n(\lambda) = \sqrt{1 + \frac{0.6961663\lambda^2}{\lambda^2 - (0.0684043 \mu\text{m})^2} + \frac{0.4079426\lambda^2}{\lambda^2 - (0.1162414 \mu\text{m})^2} + \frac{0.8974794\lambda^2}{\lambda^2 - (9.896161 \mu\text{m})^2}}. \quad (\text{A.1})$$

The material inside a Pockels cell is called potassium dideuterium phosphate (KD\*P) with the chemical formula  $\text{KD}_2\text{PO}_4$ . Its dispersion formula is [23]

$$n(\lambda) = \sqrt{1 + \frac{1.239234\lambda^2}{\lambda^2 - 0.0083531147 \mu\text{m}^2} + \frac{1478889\lambda^2}{\lambda^2 - 88511870 \mu\text{m}^2}}. \quad (\text{A.2})$$

The material most commonly used to pump the laser beam is YAG with the chemical formula  $\text{Y}_3\text{Al}_4\text{O}_{12}$ . The dispersion formula is [24]

$$n(\lambda) = \sqrt{1 + \frac{2.28200\lambda^2}{\lambda^2 - 0.01185 \mu\text{m}^2} + \frac{3.27644\lambda^2}{\lambda^2 - 282.734 \mu\text{m}^2}}. \quad (\text{A.3})$$

The refractive index  $n(\lambda)$  is depicted in figure A.1 in a range of 0.2–6  $\mu\text{m}$ . The GVD was calculated around the centre wavelength  $\lambda_0 = 1030 \text{ nm}$  and is linear in a good approximation.

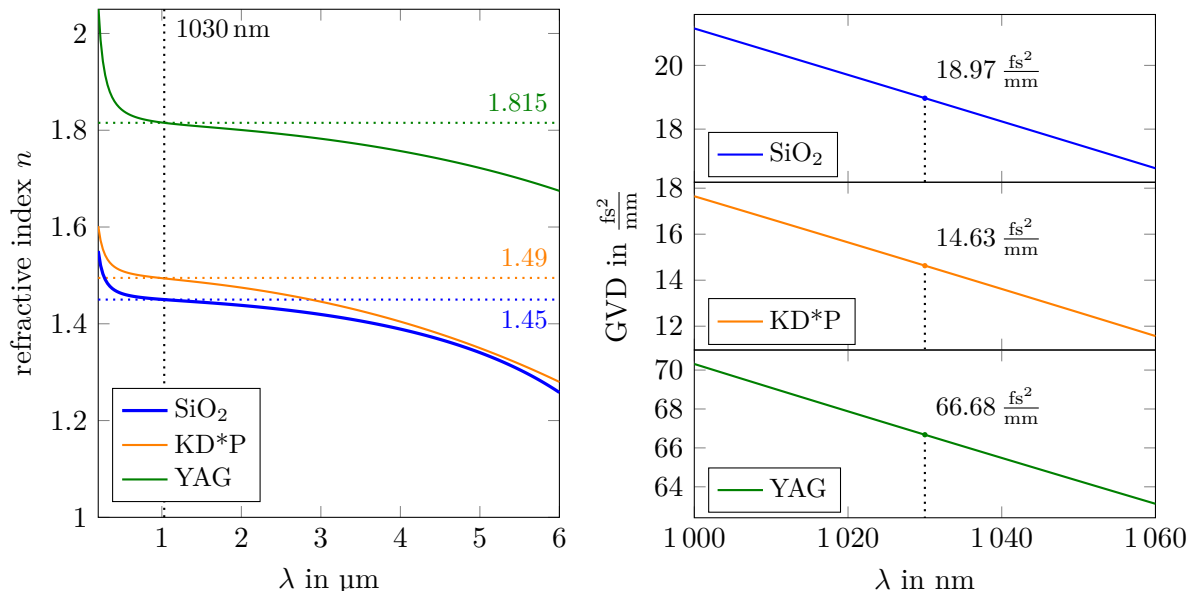


**Fig. A.1:** The left side shows the refractive index of fused silica SiO<sub>2</sub>, KD\*P (KD<sub>2</sub>PO<sub>4</sub>) and YAG (Y<sub>3</sub>Al<sub>4</sub>O<sub>12</sub>). The GVD is depicted on the right side. The value of  $n(\lambda)$  and GVD( $\lambda$ ) at 1030 nm is given for every material.

## B. Characterization of Glan-type polarizers

Other optics often used in CPA systems are polarizing prisms based on birefringence and total reflection. In conventional polarizing prisms, only one polarization direction is transmitted. This can be accomplished by cutting and cementing both halves of the prisms in such a way that the other polarization direction suffers total internal reflection at the cut. Usually it is deflected to the side of the prism. Glan type prisms have the optical axis in the plane of the entrance face [25].

The spectral phase and GDD was measured for both polarizers for p-polarized and s-polarized light. The prism were rotated for maximum transmission. The results are depicted in figure B.1.

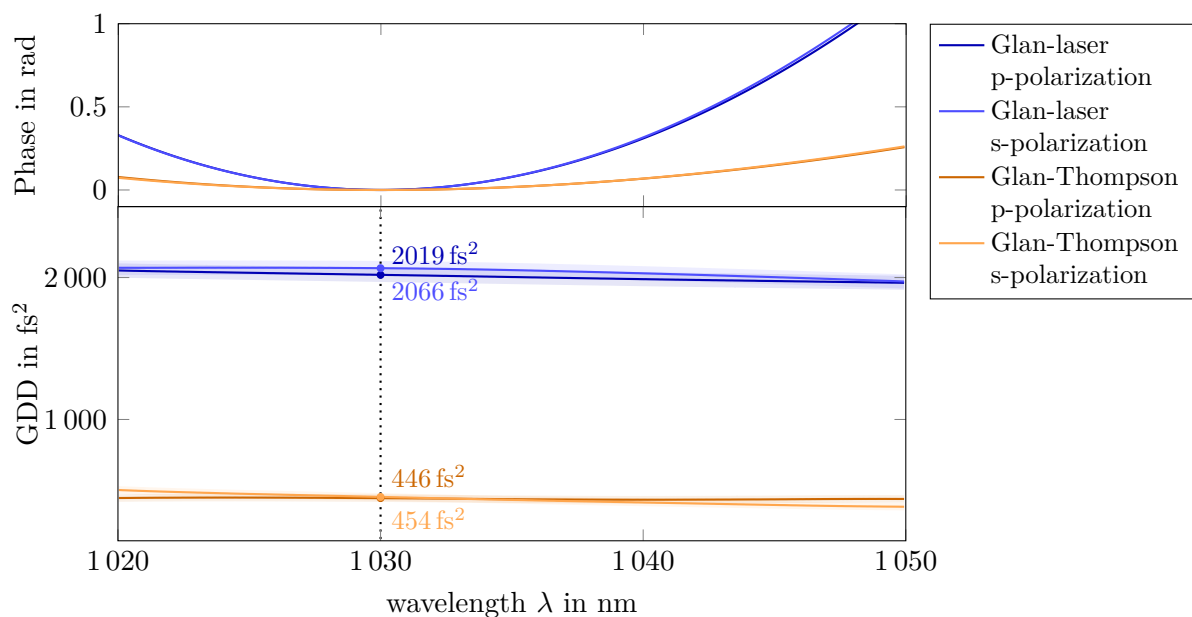


**Fig. B.1:** GDD measurement of two different polarizing prisms, a Glan-laser polarizer and Glan-Thompson polarizer, which are based on birefringence and total reflection. Both prisms were measured for p-polarization and s-polarization for a single pass of the optical component.

The phase measurements and GDD determination were made for one beam pass through the prism. Both polarization directions show no differences within the error range.

## C. The LabVIEW application

In this section the LabVIEW program developed as part of the Bachelor thesis is explained. For the creation of the program, an already existing LabVIEW visual instrument (VI) was used to display and store spectra, which is shown in figure C.1.

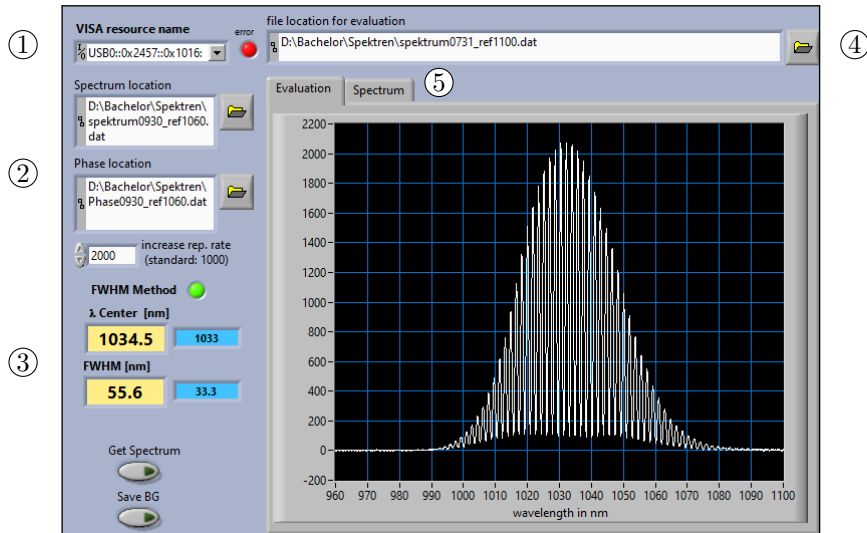


**Fig. C.1:** Data acquisition section of spectra. 1.) Selection of the spectrometer, 2.) file locations for saving the spectrum and spectral phase, 3.) centre wavelength and FWHM, 4.) file location of recorded spectra for data analysis, 5.) switch between live evaluation and recorded data analysis.

The program is able to analyze recorded spectra and evaluate live data acquisitions. It displays the centre wavelength and the FWHM. The acquired data is interpolated at equidistant frequency points (see section 4.4.4) and Fourier transformed. This is shown in figure C.2.

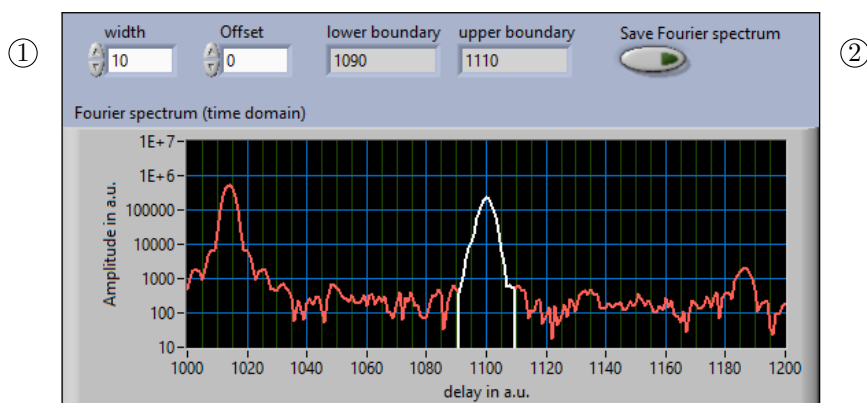


**Fig. C.2:** Fourier transform into the pseudo time domain. 1.) Selection of the window width and possible offset from the peak, 2.) Save current Fourier spectrum (red) to a file.

The spectral phase is calculated by an inverse FT of the selected data (white) in figure C.2. The spectral phase is extracted from the resulting complex values and is unwrapped. The phase is displayed in a separate panel shown in figure C.3.

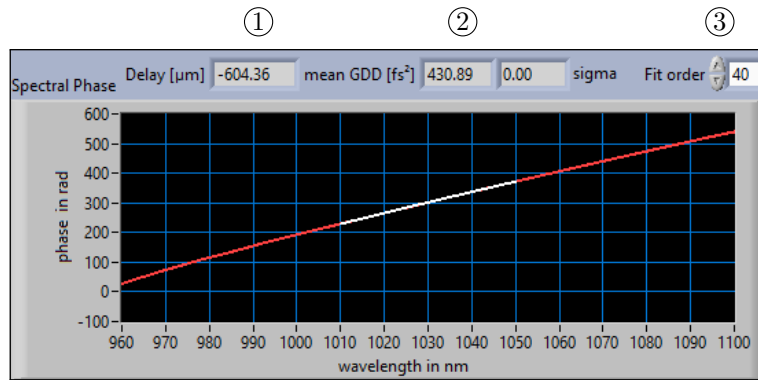


**Fig. C.3:** Spectral phase of the measured spectrum. 1.) Delay  $c \cdot t_0$  in  $\mu\text{m}$ , 2.) Averaged GDD value over 50 individual measurements with standard deviation. 3.) Order of the polynomial fit used for phase differentiation.

A polynomial of chosen order is fitted to the spectral phase and differentiated two times in a certain wavelength interval. The resulting graph in figure C.4 shows the GDD for the numerical differentiation method and the second derivative of the polynomial.

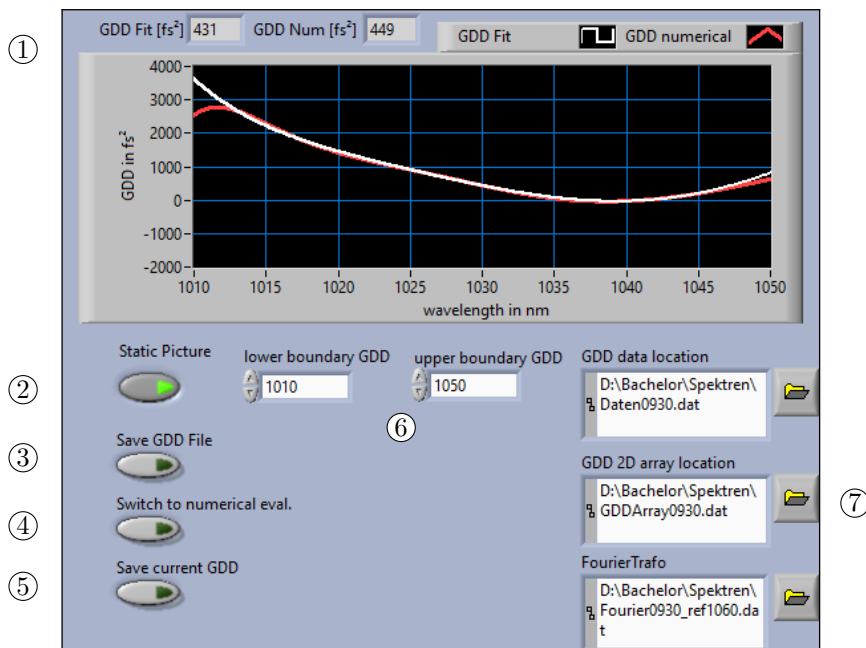


**Fig. C.4:** Retrieved GDD from the spectrum. 1.) GDD at  $\lambda_0 = 1030 \text{ nm}$  for both methods 2.) Switch between live data evaluation and data analysis of recorded spectra. 3.) Save GDD values in memory to a file. 4.) Switch of data evaluation of (3) between numerical and fitting method. 5.) Save current GDD value and its standard deviation to memory. 6.) Upper and lower boundaries for the polynomial fit. 7.) file locations.

The group delay and the third order dispersion (TOD) of the spectral phase are also displayed in separate panels.

## D. Deflection angle of a prism

The angle of deflection of a prism or a wedge shaped beam splitter can be derived geometrically with the help of figure D.1.

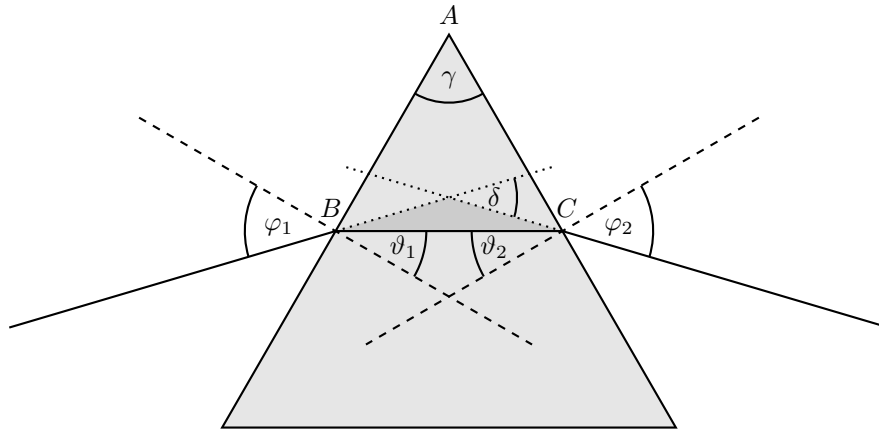


**Fig. D.1:** Beam evolution in a prism.

The dashed lines intersecting the prism at the points  $B$  and  $C$  are perpendicular to the sides of the prism. Therefore the sum of internal angles of the triangle  $ABC$  can be written as

$$\begin{aligned} 180^\circ &= (90^\circ - \vartheta_1) + (90^\circ - \vartheta_2) + \gamma \\ \Rightarrow \gamma &= \vartheta_1 + \vartheta_2. \end{aligned} \quad (\text{D.1})$$

Due to the *vertical angle theorem* the sum of internal angles of the dark shaded triangle can be written as

$$\begin{aligned} 180^\circ &= (\varphi_1 - \vartheta_1) + (\varphi_2 - \vartheta_2) + (180^\circ - \delta) \\ \Rightarrow \delta &= \varphi_1 + \varphi_2 - (\vartheta_1 + \vartheta_2) \stackrel{(\text{D.1})}{=} \varphi_1 + \varphi_2 - \gamma. \end{aligned} \quad (\text{D.2})$$

It is assumed that  $n_{\text{air}} = 1$ , therefore SNELL's law states

$$\sin \varphi_1 = n \cdot \sin \vartheta_1 \Rightarrow n \cos \vartheta_1 = \sqrt{n^2 - \sin^2 \varphi_1} \quad (\text{D.3})$$

$$\begin{aligned} \sin \varphi_2 &= n \cdot \sin \vartheta_2 \stackrel{(\text{D.1})}{=} n \cdot \sin(\gamma - \vartheta_1) \\ &= \sin \gamma \cdot (n \cos \vartheta_1) - n \cdot \sin \vartheta_1 \cos \gamma \\ &\stackrel{(\text{D.3})}{=} \sin \gamma \cdot \sqrt{n^2 - \sin^2 \varphi_1} - \sin \varphi_1 \cos \gamma. \end{aligned} \quad (\text{D.4})$$

Substituting (D.4) into (D.2) results in

$$\delta = \varphi_1 - \gamma + \arcsin \left[ \sin \gamma \sqrt{n^2 - \sin^2 \varphi_1} - \sin \varphi_1 \cos \gamma \right]. \quad (\text{D.5})$$

# **Selbstständigkeitserklärung und Veröffentlichung**

Ich erkläre, die vorliegende Bachelorarbeit selbstständig verfasst, und keine anderen als die angegebenen Quellen und Hilfsmittel verwendet zu haben. Die Bachelorarbeit ist an keiner anderen Stelle als Prüfungsleistung verwendet worden oder als Veröffentlichung erschienen.

Vonseiten des Verfassers bestehen keinerlei Einwände, diese Bachelorarbeit der Thüringer Universitäts- und Landesbibliothek zur öffentlichen Nutzung zur Verfügung zu stellen.

Jena, den 30. September 2020

---

Martin Beyer